

Expired Antifungal Drugs as Effective Corrosion Inhibitors for Carbon Steel in 1 M HCl Solution: Practical and Theoretical Approaches

Metwally Abdallah,* Kamal A. Soliman, Majda Alfakeer, Hanaa Hawsawi, Ameena Mohsen Al-bonayan, Salih S. Al-Juaid, Salah Abd El Wanees, and Mohamed S. Motawea



Cite This: *ACS Omega* 2023, 8, 34516–34533



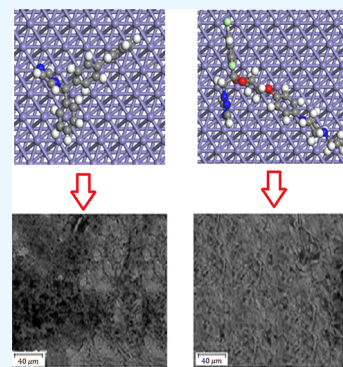
Read Online

ACCESS |

Metrics & More

Article Recommendations

ABSTRACT: The anticorrosion potency of two expired antifungal drugs, namely, bifonazole (BIF) and terconazole (TER), for X65 carbon steel (X65CS) in a 1.0 M HCl solution was estimated using practical and computational measurements. The results of all methods applied showed that the percentage of anticorrosive efficacy (% AE) increased for expired BIF and TER and reduced at elevated temperatures. The % AE values of expired BIF and TER (375 mg L^{-1}) reached 92.08 and 94.19%, respectively, using polarization methods. The anticorrosion activities of the two expired drugs were interpreted based on their adsorption on the X65CS surface. The adsorption occurred according to the Langmuir isotherm model. The polarization results indicated that the expired drugs BIF and TER were mixed inhibitors. The impedance results showed a single capacitive loop, confirming that the charge transfer process controlled the corrosion of X65CS. Expired BIF and TER served as good pitting inhibitors by shifting the pitting potential to positive values. The thermodynamic functions of activation and adsorption were defined and explained. Density functional theory and Monte Carlo simulations were used to investigate the BIF and TER inhibitors. The theoretical parameters were consistent with the experimental results. The anticorrosion efficiencies determined using the various methods were in complete agreement.



1. INTRODUCTION

Carbon steel is used in a variety of industries, including construction, roads, bridges, and petroleum. However, steel corrosion is a major problem associated with these sectors. Some strong acids are utilized to clean and remove adhered objects from these alloys. Although the acids clean steel efficiently, one disadvantage is the corrosion that occurs, causing great economic losses in most countries worldwide. Therefore, scientists have employed corrosion inhibitors to solve the corrosion problem.^{1,2}

Corrosion inhibitors minimize the corrosion rate of steel in aqueous solution and prevent carbon steel from dissolving in acidic medium. Most inhibitors are organic molecules with several active centers that accelerate the adsorption process.^{3–10} The primary mechanism for the inhibitory action of the organic molecules on the steel surface is physical or chemical adsorption. The formation of an adsorbent film isolates the steel surface from the aggressive medium.^{11–15} The inhibition strength of the organic inhibitors depend on several factors such as the electrode surface employed, the nature of aggressive solutions, the chemical composition of the additives, the physicochemical properties of the molecule with respect to the functional group, the expected steric and electronic effect of the density of donor atoms, and the possible interaction between the inhibitors with the d orbital of the iron atoms.^{16–19}

The inhibition strength depends on the amount of adsorbed layers formed, the chemical composition of the steel used, the type and concentration of the corrosive medium, the temperature, and several other factors.^{20,21}

Although these organic molecules are very effective inhibitors with reasonable inhibitory efficacy, they are not economically feasible because the cost of preparing them is very expensive and environmentally harmful.²² Therefore, the goal of this study was to use expired drugs that have no use as corrosion inhibitors for carbon steel instead of discarding and culling them, which causes innumerable economic and environmental damage. Hence, the benefit is doubled. In prior studies,^{23–30} expired drugs were utilized to inhibit the dissolution of steel in acidic media. They provided high inhibition efficiency depending on the chemical structure of the drug. The inhibition potency of expired drugs depends on their chemical structure and the presence of some

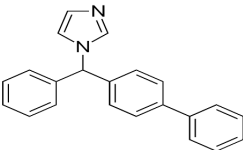
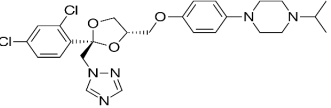
Received: May 10, 2023

Accepted: August 14, 2023

Published: September 15, 2023



Table 1. Names and Chemical Structures of Expired Antifungal Drugs Used

Name	Chemical structure	Formula and Molar mass (g mole ⁻¹)
Bifonazole (BIF)		C ₂₂ H ₁₈ N ₂ 310.400 g·mol ⁻¹
Terconazole (TER)		C ₂₆ H ₃₁ Cl ₂ N ₅ O ₃ 532.47 g·mol ⁻¹

energetic centers that facilitate the adsorption of these drugs on the metal surface.

In this study, we used expired antifungal drugs, namely bifonazole (BIF) and terconazole (TER), to inhibit corrosion of X65 carbon steel (X65CS) in 1 M HCl rather than discarding them, which causes innumerable environmental problems. Thus, the benefit is double. The inhibitory strength of these drugs was determined using mass loss (ML), galvanostatic polarization (GAP), potentiodynamic anodic polarization (PDAP), and electrochemical impedance spectroscopy (EIS) methods. Density functional theory (DFT) and Monte Carlo (MC) simulation are particularly effective techniques for computational studies to predict and model the adsorption of expired drugs on steel surfaces.^{31–33} Therefore, the present work aimed to study the effect of the structural parameters of expired BIF and TER on their AE by the most active sites of corrosion inhibitors using the electronic functions obtained from DFT calculations. Quantum chemical parameters were applied to correlate the experimental data with the theoretical parameters to determine the inhibition mechanism of these drugs.

2. EXPERIMENTAL METHODS

2.1. Measurements. The chemical composition of the X65 carbon steel (X65CS) applied in this work was: (weight %) C: 0.11, Mn: 1.18, Cr: 0.17, Mo: 0.15, Ni: 0.42, Nb: 0.023, V: 0.06, Ti < 0.01, and the remainder was Fe.

For the ML measurements, an X65CS sample with dimensions of 3 cm × 2.1 cm × 0.18 cm was furnished using different grades of sandpapers ranging from 200 to 1500, washed twice with distilled water and acetone, and then dried. The ML methods were implemented according to previous studies.³⁴

Electrochemical methods such as GAP, PDAP, and EIS were performed using an X65CS rod with an exposed bottom surface area of 0.38 cm². A three-compartment cell was used with X65CS serving as the working electrode, a saturated calomel electrode serving as the reference electrode, and Pt serving as the counter electrode. The treatment of the X65CS electrode was performed according to the ML method. For the GAP and PDAP methods, a PS remote potentiostat was used with PS6 software to determine the corrosion functions at scan rates of 2 and 0.2 mV s⁻¹, respectively. The EIS method was performed at a frequency range of 10 to 100 mHz and a signal amplitude perturbation of 5 mV utilizing a computer-controlled potentiostat (Auto Lab 30, Metrohm). All of these methods were adjusted at 24 °C ± 1 °C utilizing a thermostat.

2.2. Determination of the Percentage of Anticorrosion Efficacy (% AE). The percentages of anticorrosion efficacy (% AE) of the two expired drugs (BIF and TER) were calculated from the ML and GAP methods by applying eq 1:

$$\%AE = \left[1 - \frac{Y}{Z} \right] 100 \quad (1)$$

For the ML and GAP measurements, Y and Z are the mass loss or corrosion current density in the presence of expired BIF and TER and in the HCl solution alone, respectively. Conversely, for the impedance measurements, Y and Z are the charge transfer resistances in the HCl solution alone and in the presence of expired BIF and TER, respectively. The surface coverage (θ) was determined from eq 2:

$$\theta = \%AE/100 \quad (2)$$

2.3. Inhibitors. Two expired antifungal drugs, namely, BIF and TER, were applied as corrosion inhibitors. The drugs were manufactured by EIPICO Pharmaceutical Company, Egypt. Their structures are listed in Table 1.

2.4. Computational Approach. The computational study was conducted for the TER and BIF inhibitors using DFT. The optimized geometries were obtained through the B3LYP and 6-31 g(d,p) level of theory in the aqueous phase. The conductor-like polarizable continuum model was employed for the solvent effect.³⁵ The calculations were implemented in the Gaussian 09 code.³⁶ Some parameters, such as the energies of the highest occupied molecular orbital (E_{HOMO}) and lowest unoccupied molecular orbital (E_{LUMO}), energy gap (ΔE), global softness (σ), hardness (η), and the fraction of electrons transferred (ΔN), were calculated as follows.

$$\eta = \frac{E_{\text{LUMO}} - E_{\text{HOMO}}}{2} \quad (3)$$

$$\sigma = \frac{1}{\eta} \quad (4)$$

$$\Delta N = \frac{\phi - \chi_{\text{inh}}}{2(\eta_{\text{Fe}} + \eta_{\text{inh}})} \quad (5)$$

where ϕ (the work function of iron) = 4.82 eV³⁷ and $\eta_{\text{Fe}} = 0$.

The Fukui index indicates the potential site on the inhibitor molecules where electrophilic or nucleophilic attacks can occur. The following formulas are used to calculate the Fukui index for

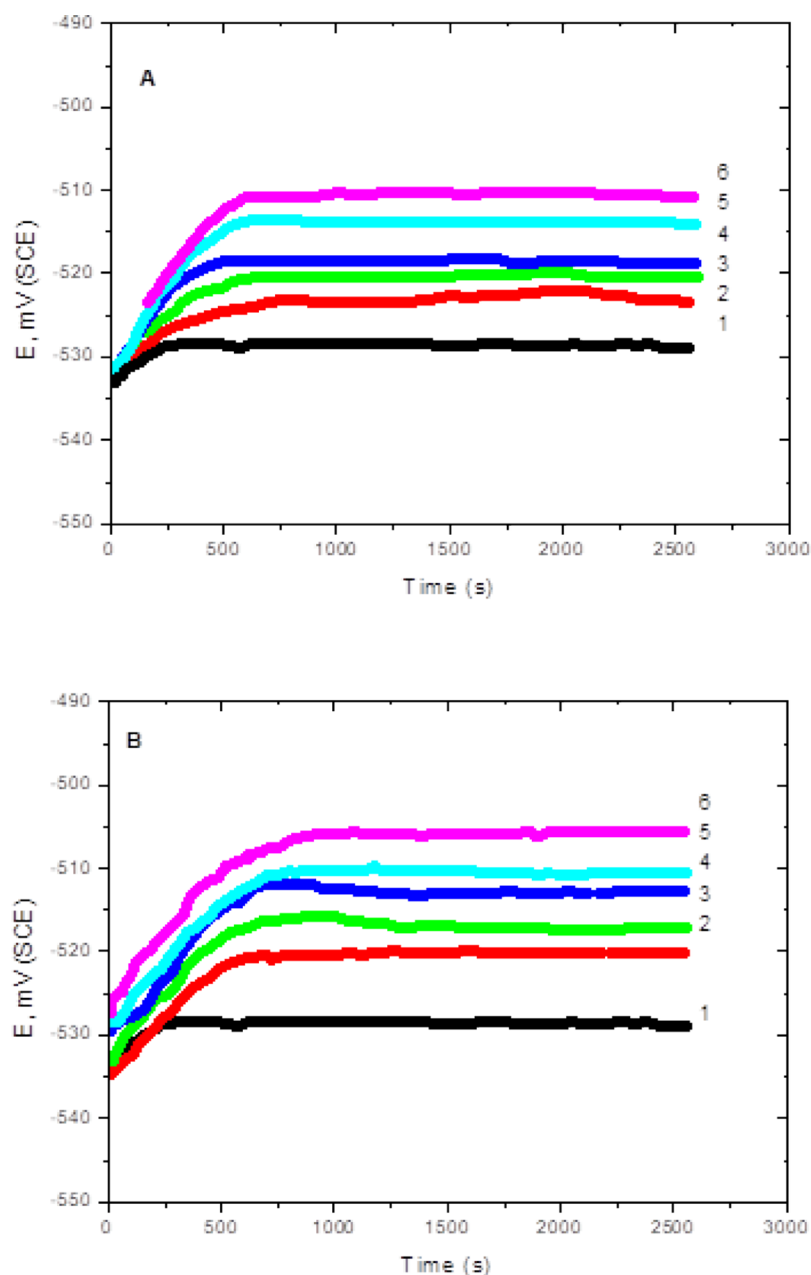


Figure 1. (A, B) Relationship between the OCP vs time curves for X65CS corrosion in 1 M HCl with and without different concentrations of the (A) BIF drug and (B) TER drug. (1) 0.0 mg L⁻¹, (2) 75 mg L⁻¹, (3) 150 mg L⁻¹, (4) 225 mg L⁻¹, (5) 300 mg L⁻¹, and (6) 375 mg L⁻¹.

both nucleophilic (f^+) and electrophilic (f^-) attacks using the Mulliken population analysis.

$$f^+ = q(N + 1) - q(N) \quad (6)$$

$$f^- = q(N) - q(N - 1) \quad (7)$$

where $q(N + 1)$, $q(N)$ and $q(N - 1)$ are the charges of the atoms present in the system with $N + 1$, N , and $N - 1$ electrons, respectively.

2.5. Monte Carlo Simulation. The MC simulation was implemented to explore the interaction of the TER and BIF molecules using the adsorption locator module in the Material Studio 2017 code on the Fe (110) surface.³⁸ The computations were conducted using a simulation box of 32.27 Å × 32.27 Å × 33.10 Å. To calculate the lowest adsorption energy (E_{ads}) for the inhibitors on the Fe (1 1 0) surface, the COMPASS force field

and an atom-based simulation technique were used. The E_{ads} arising from the interaction of the TER and BIF inhibitors with the Fe (110) substrate was evaluated by eq 8

$$E_{\text{ads}} = E_{\text{total}} - E_{\text{Fe}(110)} - E_{\text{inh}} \quad (8)$$

where E_{total} , $E_{\text{Fe}(110)}$, and E_{inh} are the overall energy of the expired drug and the Fe (110) surface, the energy of Fe (110), and the energy of the drug molecule, respectively.

3. RESULTS AND DISCUSSION

3.1. GAP Methods. Figure 1A,B depicts the OCP versus time curves for X65CS corrosion in 1 M HCl in the absence and presence of various concentrations of expired BIF and TER. A steady-state potential was attained soon after it was recorded. This illustrates that the surface oxide layer was completely dissolved when the metal specimen was submerged in the

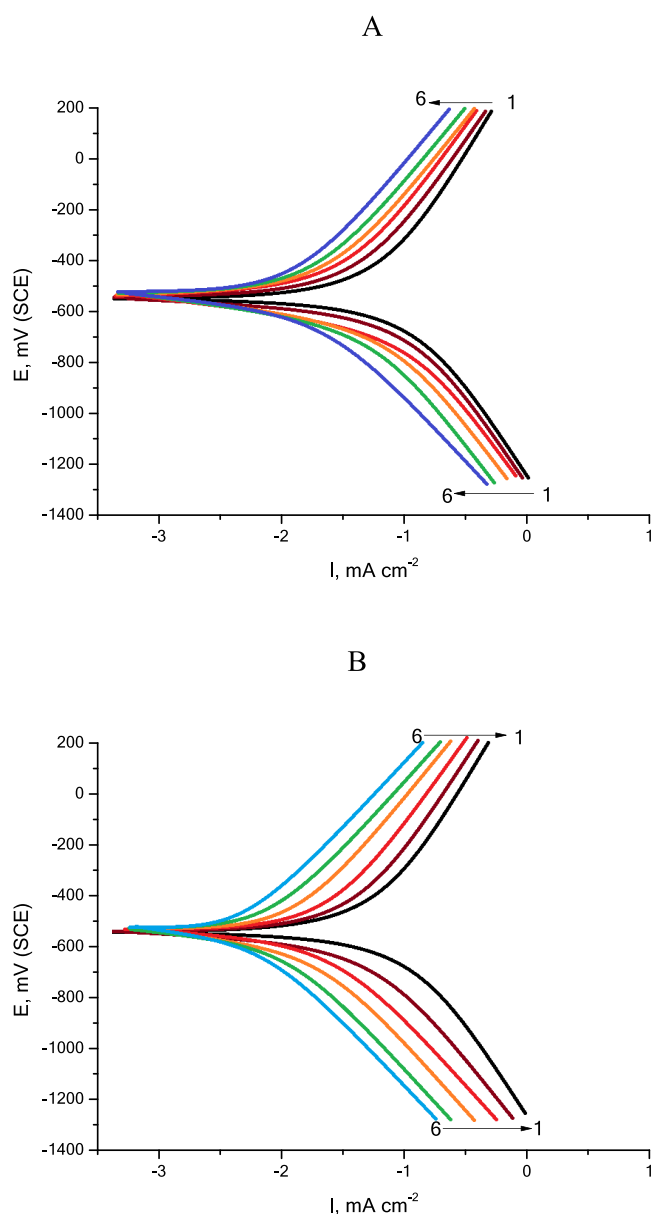


Figure 2. (A, B) GAP curves for the corrosion of X65CS in 1 M HCl alone and with diverse concentrations of the (A) BIF drug and (B) TER drug. (1) 0.0 mg L⁻¹, (2) 75 mg L⁻¹, (3) 150 mg L⁻¹, (4) 225 mg L⁻¹, (5) 300 mg L⁻¹, and (6) 375 mg L⁻¹.

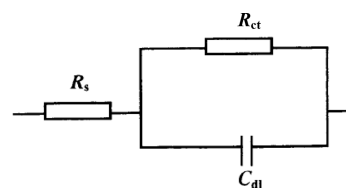


Figure 3. Electrochemical equivalent circuit applied to fit the EIS parameters.

electrolyte for 2500 s. The OCP for the two expired BIF and TER concentrations moves toward the positive direction. This suggests that the expired BIF and TER function by getting adsorbed at the steel/solution interface.³⁹

Figure 2A,B presents the GAP curves for X65CS 1M HCl solution including the diverse concentration of expired drugs BIF and TER, respectively.

The corrosion functions were derived from Figure 1 such as the current density (I_{corr}), corrosion potential (E_{corr}), anodic and cathodic Tafel slopes (β_a and β_c), and anticorrosion efficacy (% AE) and are listed in Table 2. Clearly, from Table 2, increasing the concentration of expired drugs indicates the following:

- (i) The acquired anodic and cathodic exhibit Tafel behavior. The augmentation of the BIF and TER drugs increased both cathodic and anodic overvoltages and essentially caused parallel shifts to the more negative and positive values, respectively, for free curves. Thus, these expired drugs affect the cathodic and anodic operations. This means that these examined drugs reduce the H₂ evolution reaction and the anodic dissolution reaction of X65CS. These outcomes indicate these expired drugs as mixed-type inhibitors.
- (ii) Values of β_a and β_c have been altered, but the values of β_a more than β_c demonstrate that the expired BIF and TER serving as mixed inhibitors are mostly anodic ($\beta_a > \beta_c$).
- (iii) Values of E_{corr} moving a little bit to a more negative direction. The shift in E_{corr} in the case of an expired BIF is equal to 18 mV and 23 mV in the case of expired Ter. This confirms that these two expired drugs were categorized as mixed inhibitors.^{40,41}
- (iv) The values of I_{corr} reduced and increased the % AE demonstrating the inhibitory activity of the two drugs. In all concentrations used, the % AE of the TER drug is more than that of the BIF drug. Its value at 375 mg L⁻¹ reached 94.19% in TER, while it reached 92.08% in the BIF drug.

Table 2. Electrochemical Parameters Obtained from GAP of X65CS in 1 M HCl Including Certain Doses of Expired BIF and TER at 26 °C

medium	inh. conc. (mg L ⁻¹)	$-\beta_c$ (mV dec ⁻¹)	β_a (mV dec ⁻¹)	$-E_{\text{corr}}$ (mV) (SCE)	I_{corr} (mA cm ⁻²)	$R_p \times 10^2$ (Ω cm ²)	% AE
blank	0	726	834	528	12.75	1.75	
BIF	75	626	765	523	4.22	3.12	66.90
	150	588	734	520	3.36	3.30	73.65
	225	562	703	518	2.48	3.46	80.55
	300	535	685	513	1.36	3.58	89.33
	375	505	652	510	1.01	3.64	92.08
TER	75	637	745	520	3.55	3.31	72.16
	150	590	712	516	2.79	3.43	78.12
	225	564	684	512	2.12		83.37
	300	523	652	510	1.05		91.76
	375	495	628	505	0.74	3.72	94.19

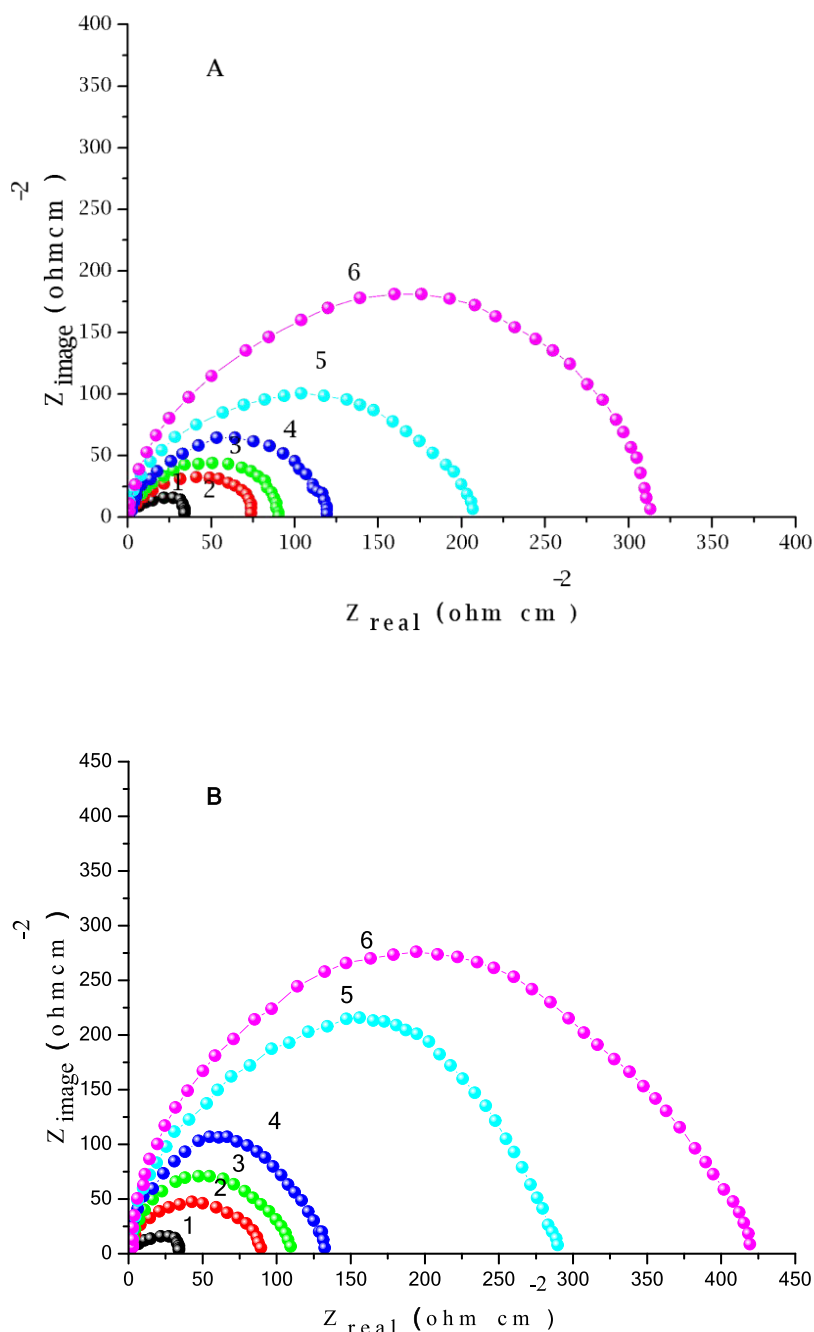


Figure 4. (A, B) Nyquist plots of X65CS in 1.0 M HCl in 1 M HCl alone and with diverse concentrations of the (A) BIF drug and (B) TER drug. (1) 0.0 mg L⁻¹, (2) 75 mg L⁻¹, (3) 150 mg L⁻¹, (4) 225 mg L⁻¹, (5) 300 mg L⁻¹, and (6) 375 mg L⁻¹.

(v) The values of R_p increases from 175 to 364 ohm for BIF and 372 ohm for TER, respectively.

3.2. EIS Measurements. The corrosion behavior of X65CS was investigated using EIS measurements at 26 °C in 1 M HCl alone and with certain concentrations of expired BIF and TER. Two major diagram formats, namely, the Nyquist and Bode formats, are often used to display EIS data. In a Nyquist diagram, the real component of the impedance is plotted versus the imaginary component at various frequencies. The solution resistance (R_s) and charge transfer resistance (R_{ct}) values are determined from the intersection of the semicircle with the real component axis.

The capacitance of the double layer (C_{dl}) was calculated from the angular frequency ($\omega = 2\pi f$) at the maximum imaginary component and R_{ct} values, utilizing the following equation

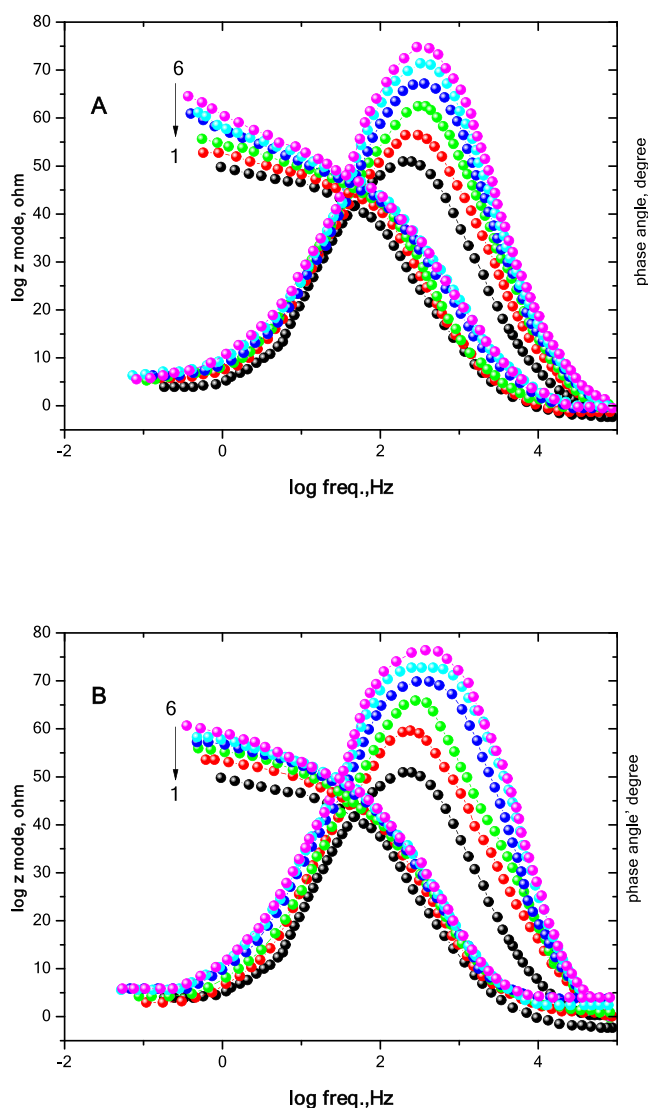
$$C_{dl} = \frac{1}{\omega_{max} R_{ct}} = \frac{1}{2\pi f_{max} R_{ct}} \quad (9)$$

where f is the frequency of the electrochemical circuit applied in the EIS analysis (Figure 3).

The Nyquist diagrams of X65CS in the 1 M HCl solution with different concentrations of expired BIF and TER are displayed in Figure 4A,B. Because of the rough and inhomogeneous X65CS surface, the impedance plot does not show idealistic semicircles due to the frequency dispersion.^{42,43} The radii of the semicircles increased as the concentrations of expired BIF and TER

Table 3. EIS Parameters for X65CS in Free 1 M HCl Solution and Containing Certain Doses of Expired BIF and TER Drugs

medium	inh. conc. (mg L ⁻¹)	R _s (Ω cm ²)	C _{dl} (μF cm ⁻²)	R _{ct} (Ω cm ²)	% AE
blank	0.00	1.66	102.05	25	
BIF	75	1.84	89.12	71	64.78
	150	1.88	78.43	88	71.59
	225	1.96	69.81	115	78.26
	300	2.09	60.83	205	87.80
	375	2.21	54.37	310	91.93
TER	75	1.98	81.54	86	70.93
	150	2.08	74.52	107	76.63
	225	2.18	66.35	130	80.76
	300	2.22	59.22	285	91.22
	375	2.28	51.84	425	94.12

**Figure 5.** (A, B) Bode plot of X65CS in 1 M HCl devoid of and containing diverse concentrations of the (A) BIF drug and (B) TER drug. (1) 0.0 mg L⁻¹, (2) 75 mg L⁻¹, (3) 150 mg L⁻¹, (4) 225 mg L⁻¹, (5) 300 mg L⁻¹, and (6) 375 mg L⁻¹.

increased, demonstrating the protective features of the X65CS and the charge transfer operation that fundamentally controls the dissolution of X65CS.^{44,45}

The EIS functions, namely, R_s, C_{dl}, R_{ct}, and % AE, are shown in Table 3. The C_{dl} values decreased as the concentration of expired BIF and TER increased because the water molecules on the surface were progressively replaced by the expired-drug molecules. These drug molecules formed a layer on the X65CS surface, which minimized the local dielectric constant of the X65CS/solution interface. Owing to the creation of an adhesive layer at the X65CS/solution interface, the R_{ct} values increased and thus the % AE values increased.

The Bode and phase angle diagrams showing the effect of various BIF and TER concentrations on the corrosion of X65CS in 1 M HCl are presented in Figure 5A,B. In the impedance diagrams, the magnitude increased at lower frequencies because of the enhanced protection with the increased BIF and TER concentrations, which was attributed to the adsorption of BIF and TER on the X65CS surface.⁴⁶ The phase angle diagram showed that increasing the expired-drug concentrations resulted in superior inhibitory performance because of greater adsorption on the X65CS surface. Moreover, the phase angle at the relaxation frequency decreased with decreasing expired-drug concentrations, indicating the reduced capacitive response at lower drug concentrations. In the same concentrations, the % AE of TER was higher than that of BIF.

3.3. PDAP Measurement. Expired BIF and TER were tested as pitting corrosion inhibitors utilizing the PDAP measurements. The PDAP of X65CS in 1 M HCl + 0.5 M NaCl containing different concentrations of expired BIF and TER at a sweep rate of 0.1 mV s⁻¹ are shown in Figure 6A,B. This figure shows that, as the potential increased, the current remained constant, indicating the stability of the passive film on the X65CS. At a specific potential, the Cl⁻ ions were able to penetrate the passive film and the current increased quickly. This potential is known as the pitting potential (E_{pitting}).^{20,47} E_{pitting} moved to positive values with higher concentrations of expired BIF and TER, indicating the increased resistance of X65CS to pitting attacks using expired BIF and TER as pitting inhibitors.

The plots between E_{pitting} and the logarithm of the concentrations of expired BIF and TER are presented in Figure 7. Straight lines were obtained, and with higher concentrations of expired BIF and TER, the E_{pitting} values showed a positive trend according to the following relationship^{23,48}

$$E_{\text{pitting}} = \partial + \alpha \log C_{\text{ex-drugs}} \quad (10)$$

where ∂ and α are constants that depend on the type of the working electrode and inhibitors used (the units of ∂ is mV and the unit of α is mV/(mg L)). These results demonstrate that the expired BIF and TER served as inhibitors of X65CS pitting corrosion. In the case of expired TER, the positive shift in E_{pitting} was greater than that obtained for BIF, demonstrating that expired TER had a greater ability to inhibit pitting corrosion than expired BIF.

3.4. ML Methods. **3.4.1. Effect of Expired-Drug Concentrations.** The effect of some concentrations of expired BIF and TER (75, 150, 225, 300, and 375 mg L⁻¹) on the corrosion of X65CS in 1 M HCl was evaluated utilizing ML measurements. The corrosion rate (K_{corr}) depends on the X65CS surface area (S) and the inundation time (t) according to the following relation^{49,50}

$$K_{\text{corr}} = \frac{ML}{S \cdot t} \quad (11)$$

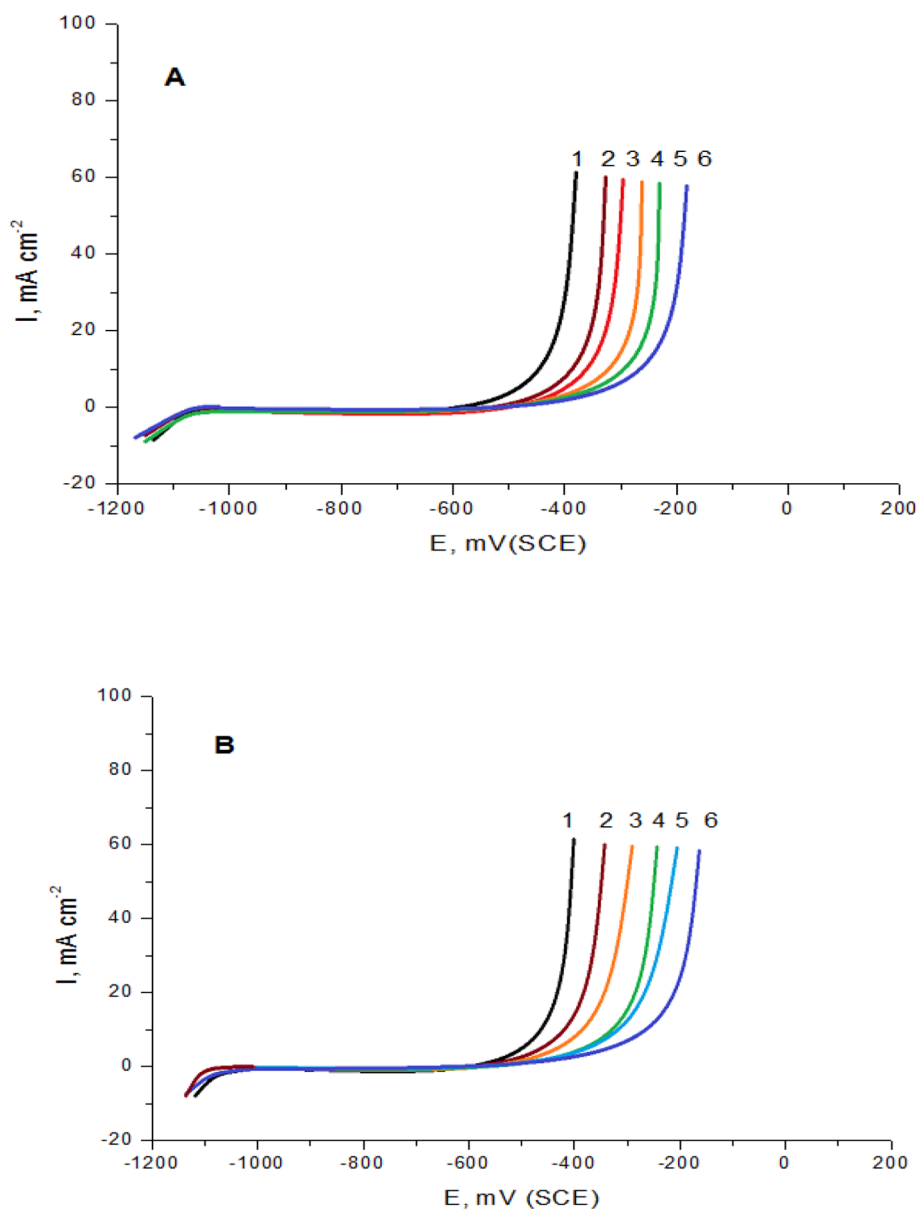


Figure 6. (A, B) PDAP curves of carbon steel in X6SCS in 1 M HCl solution + 0.5 M NaCl and also when containing certain concentrations of expired (A) BIF and (B) TER at a scan rate of 1 mV s^{-1} . (1) 0.00, (2) 75, (3) 150, (4) 225, (5) 300, and (6) 375 mg L^{-1} .

where $ML = M_a - M_b$, M_a and M_b are the ML before and after immersion in the tested electrolyte, respectively (the unit of K_{corr} is $\text{mg cm}^{-1} \text{ min}^{-1}$).

The ML, K_{corr} , % AE, and θ values of the expired BIF and TER at 299 K are shown in Tables 4A and 4B, respectively. As the concentrations of expired BIF and TER increased, the ML decreased and the values of % AE and θ increased, confirming the anticorrosive strength of these drugs. The % AE values of BIF and TER at 300 mg L^{-1} were 90.15 and 91.88, respectively. The % AE results were consistent with those obtained in the GAP and EIS measurements.

3.4.2. Effect of Elevated Temperatures. The effect of elevated temperatures from 299 to 329 K on the corrosion of X6SCS in 1.0 M HCl solution was examined using the ML method with different concentrations of expired BIF and TER (Tables 4A and 4B). With the increase in the temperature, the ML and K_{corr} increased, and thus the θ and % AE values decreased. The decrease in the % AE values was a result of the

adsorbed expired drugs being removed from the X6SCS surface at high temperatures. These results indicate that the adsorption of expired BIF and TER on the X6SCS surface is physical.

3.4.3. Computation of Thermodynamic Activation Coefficients. The activation energy (E_a^*), enthalpy of activation (ΔH^*), and entropy of activation (ΔS^*) for the dissolution of X6SCS in 1 M HCl and in the presence of different concentrations of expired BIF and TER were determined from the Arrhenius-type equation and transition-state relations as follows^{51,52}

$$K_{\text{corr}} = Ae^{(-E_a/RT)} \quad (12)$$

$$K_{\text{corr}} = \frac{RT}{Nh} e^{(\Delta S^*/R)} e^{(-\Delta H^*/RT)} \quad (13)$$

where A is the frequency factor, N is Avogadro's number, and h is the Planck's constant.

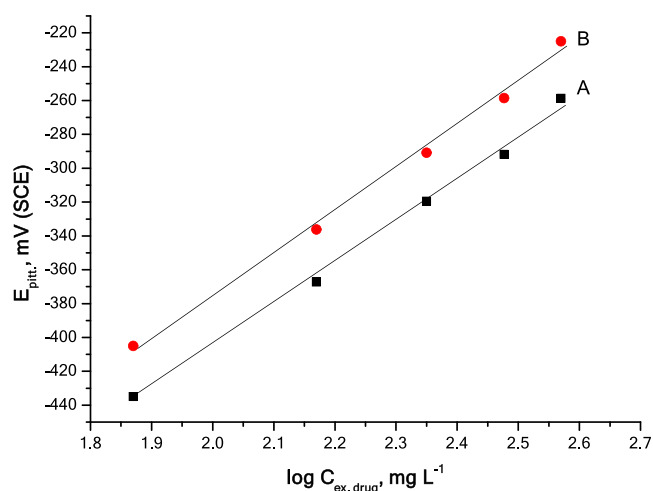


Figure 7. Relationship between the pitting potential and logarithm concentrations of expired drug: (A) BIF and (B) TER.

E_a^* values were determined from the slopes of the diagram between $\log K_{\text{corr}}$ and $1/T$ for the dissolution of X65CS in 1 M HCl solution alone, and the existence of diverse concentrations of expired BIF and TER is displayed in Figure 8A,B. Straight lines with a slope equal to $-E_a^*/2.303R$. E_a^* values are shown in Table 5. Evidently, the E_a^* values augment with the augmentation of the concentrations of expired BIF and TER. This elucidate the vigor absorption of the two expired drugs on the X65CS surface and demonstrates the energy barrier induced by the adsorption of expired BIF and TER on the steel surface.

Figure 9A,B presents the graph between $\log K_{\text{corr}}/T$ and $1/T$ for the dissolution of X65CS in 1 M HCl solution alone and the existence of certain concentrations of expired BIF and TER.

Straight lines are acquired. The values ΔH^* and ΔS^* were determined from the slopes and the intercepts of the straight lines and are registered in Table 5. Clearly, the values of ΔH^* rises with rising concentrations of expired BIF and TER, indicating that the addition of the expired drugs to a free 1 M HCl solution raising the energy barrier for the corrosion reaction relies on the nature, structure, and concentration of the investigated expired drugs. Also, the positive label of ΔH^* demonstrates that the dissolution of X65CS in 1 M HCl solution is endothermic in nature. The ΔS^* values in HCl solution and in the occurrence of expired BIF and TER are large and negative, demonstrating that the activated complex represents binding instead of disengagement.⁵³ The sequence of the anticorrosion efficacy of expired BIF and TER as obtained from the augmented E_a^* and ΔH^* values and reduced ΔS^* values are in this sequence: TER > BIF.

3.5. Surface Morphology. Figure 10A,B displays the SEM micrographs of the X65CS surface in 1 M HCl solution before immersion in 1 M HCl and after immersion for an interval of 5 h in the 1 M HCl free of any inhibitors, respectively. The micrograph in Figure 11A exhibits a smooth surface free from any corrosion damage due to the absence of Cl^- ions. The micrographs in Figure 11B depict the appearance of the X65CS after immersion in 1 M HCl for an interval extending to 5 h at 25 °C. A corroded surface appears with corrosion products contaminating it as a result of the corrosive nature of Cl^- ions.

The micrographs in Figure 10C,D depict the state of the X65CS surface when 500 ppm BIF and TER is added, respectively. Less destructive surfaces with very fine pits contaminated by corrosion products are observed due to the inhibition influence of the used inhibitors. The surface appears to be less affected in the micrograph in Figure 11D,

Table 4A. Influence of Elevating the Temperature on the Corrosion Parameters Acquired from WR Measurements for Corrosion X65CS in 1 M HCl Devoid of and Containing Diverse Concentrations of the Expired BIF Drug

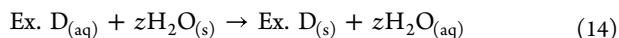
temp (K)	concn of BIF (mg L ⁻¹)	ML (mg)	$K_{\text{corr}} \times 10^{-4} \text{ h}^{-1} \cdot \text{mg cm}^{-2}$	θ	AE _(WR) %
299	0.00	0.345	11.733		
	75	0.131	4.455	0.620	62.03
	150	0.106	3.605	0.693	69.27
	225	0.082	2.788	0.762	76.24
	300	0.051	1.734	0.852	85.22
	375	0.034	1.156	0.901	90.15
309	0.00	0.438	14.89		
	75	0.176	5.985	0.598	59.80
	150	0.195	5.548	0.627	62.74
	225	0.118	4.013	0.730	73.05
	300	0.085	2.891	0.806	80.58
	375	0.065	1.963	0.868	86.82
319	0.00	0.547	18.620		
	75	0.246	8.366	0.551	55.07
	150	0.235	7.992	0.571	57.08
	225	0.175	5.952	0.680	68.03
	300	0.136	4.625	0.752	75.16
	375	0.111	3.334	0.821	82.09
329	0.00	0.638	21.698		
	75	0.313	10.654	0.509	50.89
	150	0.293	9.973	0.540	54.04
	225	0.226	7.693	0.645	64.54
	300	0.197	6.706	0.691	69.09
	375	0.147	4.765	0.780	78.04

Table 4B. Influence of Elevating the Temperature on the Corrosion Parameters Acquired from WR Measurements for Corrosion X65CS in 1.0 M HCl Devoid of and Containing Diverse Concentrations of the Expired TER Drug

temp (K)	concn of TER (mg L ⁻¹)	WR (mg)	$K_{\text{corr}} \times 10^{-4} \text{ h}^{-1} \cdot \text{mg cm}^{-2}$	θ	AE _(WR) %
299	0.00	0.345	11.733		
	75	0.103	3.503	0.701	70.14
	150	0.083	2.823	0.759	75.94
	225	0.067	2.279	0.806	80.58
	300	0.038	1.292	0.889	88.98
	375	0.028	0.952	0.919	91.88
309	0.00	0.438	14.890		
	75	0.145	4.931	0.669	66.88
	150	0.123	4.183	0.719	71.91
	225	0.105	3.571	0.760	76.02
	300	0.072	2.451	0.835	83.54
	375	0.056	1.906	0.872	87.19
319	0.00	0.547	18.620		
	75	0.207	7.040	0.623	62.19
	150	0.181	6.156	0.669	66.94
	225	0.153	5.203	0.721	72.06
	300	0.109	3.707	0.801	80.09
	375	0.087	2.959	0.857	85.73
329	0.00	0.638	21.698		
	75	0.268	9.115	0.580	57.99
	150	0.242	8.230	0.621	62.07
	225	0.204	6.938	0.680	68.02
	300	0.147	4.999	0.770	76.96
	375	0.121	4.115	0.810	81.04

demonstrating that TER is a more effective inhibitor than BIF against the corrosion of X65CS in 1 M HCl solutions.

3.6. Adsorption Performance and Corrosion Prevention Mechanism. The expired BIF and TER reduced X65CS corrosion in a 1 M HCl solution mainly by their adsorption on the X65CS surface. Adsorption can be considered an exchange process in which an amount (z) of H₂O molecules adsorbed on the X65CS surface ($z\text{H}_2\text{O}_{(s)}$) is replaced with expired drugs (Ex.D) from the aqueous solution according to eq 14:



The adsorption strengths of expired BIF and TER depend on the chemical structure and the presence of active centers facilitating the adsorption of the drugs on the steel surface. Additionally, the chemical constituents of the steel applied in this study, the concentration of aggressive acids, and the temperature affect the adsorption strength. Furthermore, the adsorption provides information on the interactions of the adsorbent species with one another and with the X65CS surface. Several adsorption isotherms have been compared to the data obtained from the ML method to select the best isotherm. We found that the best isotherm matching the present data follows the Langmuir isotherm according to eq 15

$$C_{\text{ex-drug}} + \frac{1}{K_{\text{ads}}} = \frac{C_{\text{ex-drug}}}{\theta} \quad (15)$$

where $C_{\text{ex-drug}}$ is the concentration of the expired drug and K_{ads} is the equilibrium constant of adsorption.

Figure 11A,B presents the Langmuir plots ($C_{\text{ex-drug}}/\theta$ and $C_{\text{ex-drug}}$) of the adsorption of the two expired drugs (BIF and TER) on the X65CS surface in a 1 M HCl solution at various temperatures (299, 309, 319, and 329 K). The straight lines with unit slopes acquired from these diagrams indicate that the Langmuir isotherm is a suitable model. This demonstrates that

there was no reaction between adsorbed particles on the X65CS surface.

The K_{ads} values of the expired drugs (BIF and TER) were determined from the intercept of the relationship in Figure 11. The K_{ads} values of expired BIF determined from Figure 11A were 11.12×10^{-3} , 9.52×10^{-3} , 8.36×10^{-3} , and $7.14 \times 10^{-3} \text{ mol L}^{-1}$ at temperatures of 26, 36, 46, and 56 °C, respectively. The K_{ads} values of expired TER determined from Figure 11B were 16.6×10^{-3} , 12.5×10^{-3} , 10.2×10^{-3} , and $9.09 \times 10^{-3} \text{ mol L}^{-1}$ at temperatures of 26, 36, 46, and 56 °C, respectively. The high K_{ads} values demonstrate that the expired BIF and TER were easily and strongly adsorbed onto the X65CS surface.

The K_{ads} values are related to the standard free energy of adsorption ($\Delta G_{\text{ads}}^\circ$) by the following equation:^{54,55}

$$K_{\text{ads}} = \frac{1}{55.5} e^{(-\Delta G_{\text{ads}}^\circ/RT)} \quad (16)$$

The calculated $\Delta G_{\text{ads}}^\circ$ values in the presence of expired BIF were -34.24 , -32.55 , -30.99 , and $-29.02 \text{ kJ mol}^{-1}$ at temperatures of 26, 36, 46, and 56 °C, respectively. The $\Delta G_{\text{ads}}^\circ$ values in the presence of expired TER were -35.03 , -33.12 , -32.67 , and $-30.59 \text{ kJ mol}^{-1}$ at temperatures of 26, 36, 46, and 56 °C, respectively. The $\Delta G_{\text{ads}}^\circ$ values were negative, confirming that the adsorption of expired BIF and TER onto the X65CS surface was spontaneous and highly efficient.

Previous studies^{56,57} indicate that $\Delta G_{\text{ads}}^\circ$ values up to -20 kJ mol^{-1} are consistent with electrostatic interactions of the charged drug and the charged steel (indicating physical absorption), whereas values that are more negative than -40 kJ mol^{-1} are consistent with charge sharing or transfer from the expired-drug molecules to the steel surface to construct a coordinated bond (indicating chemical adsorption). The $\Delta G_{\text{ads}}^\circ$ values of the two expired drugs ranged from 33 to 38 kJ mol^{-1} , confirming that the adsorption of BIF and TER on the X65CS in

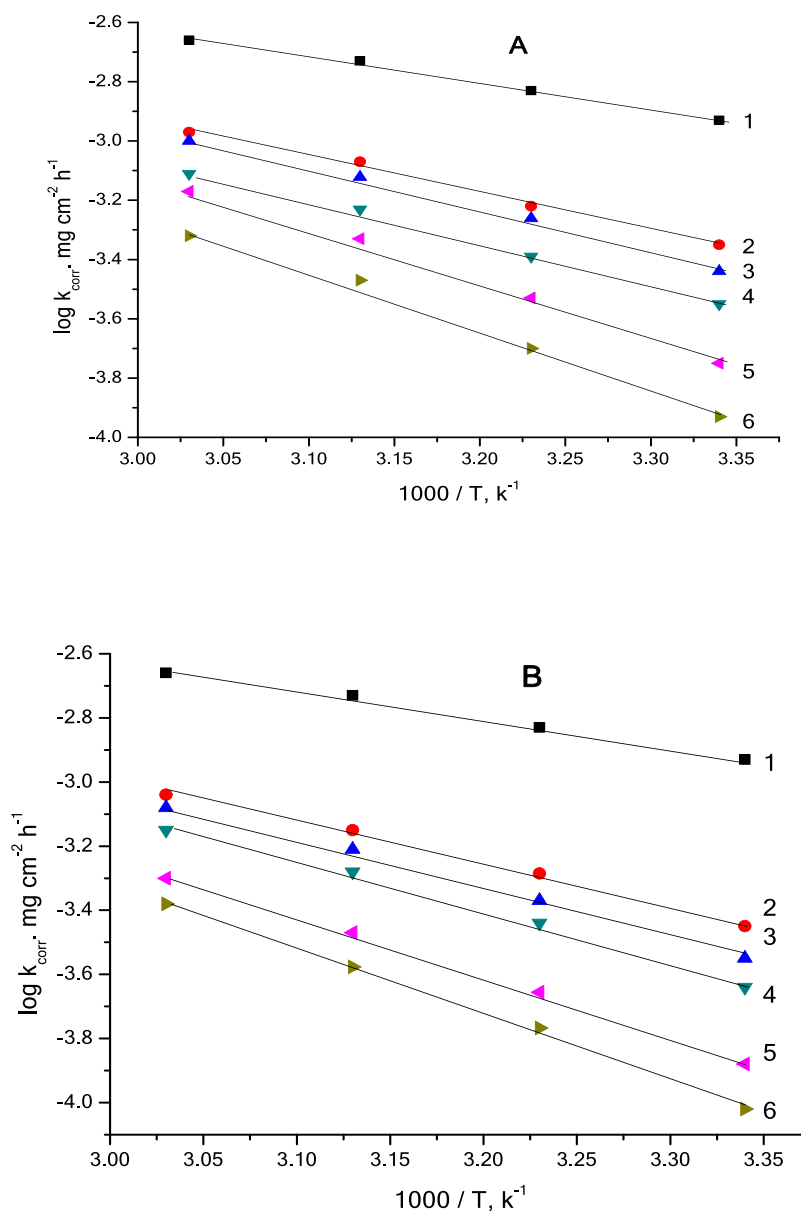


Figure 8. (A, B) Relationship between $\log K_{\text{corr}}$ and $1/T$ for the dissolution of X65CS in 1 M HCl solution alone and in the presence of some concentrations of expired (A) BIF and (B) TER. (1) 0.0 mg L⁻¹, (2) 75 mg L⁻¹, (3) 150 mg L⁻¹, (4) 225 mg L⁻¹, (5) 300 mg L⁻¹, and (6) 375 mg L⁻¹.

Table 5. Activation Thermodynamics Functions for X65CS in the Blank 1.0 M HCl Solution and in the Presence of Certain Concentrations of BIF and TER

concn of inh. (mg L ⁻¹)	E_a (kJ mol ⁻¹)	ΔH^* (kJ mol ⁻¹)	$-\Delta S^*$ (J mol ⁻¹ K ⁻¹)
1.0 M HCl	19.14	17.23	294.22
1.0 M HCl + 75 mg L ⁻¹ BIF	27.75	22.98	312.78
1.0 M HCl + 150 mg L ⁻¹ BIF	29.66	26.81	336.12
1.0 M HCl + 225 mg L ⁻¹ BIF	32.58	28.73	353.54
1.0 M HCl + 300 mg L ⁻¹ BIF	35.41	32.55	375.66
1.0 M HCl + 375 mg L ⁻¹ BIF	36.37	34.47	398.26
1.0 M HCl + 75 mg L ⁻¹ TER	28.71	27.76	316.75
1.0 M HCl + 150 mg L ⁻¹ TER	31.01	30.64	350.90
1.0 M HCl + 225 mg L ⁻¹ TER	32.08	31.59	374.22
1.0 M HCl + 300 mg L ⁻¹ TER	36.36	33.51	396.78
1.0 M HCl + 375 mg L ⁻¹ TER	38.28	37.34	424.13

1 M HCl involved a mixture of physical and chemical adsorption.^{58,59}

The enthalpy of adsorption (ΔH_{ads}) was determined using the following equation⁶⁰

$$\log K_{\text{ads}} = \frac{-\Delta H_{\text{ads}}^{\circ}}{2.303RT} + C \quad (17)$$

where C is constant. The correlations between $\log K_{\text{ads}}$ and $1/T$ for the adsorption of expired BIF and TER on X65CS in 1.0 M HCl solution are depicted in Figure 12 as straight lines. From the slope of the straight lines, the ΔH_{ads} values were determined as -11.49 and -17.23 kJ mol⁻¹ for expired BIF and TER, respectively. These values demonstrate that the adsorption of expired BIF and TER onto the X65CS surface in 1.0 M HCl was an exothermic process.

The entropy of adsorption (ΔS_{ads}) was calculated using the following equation:

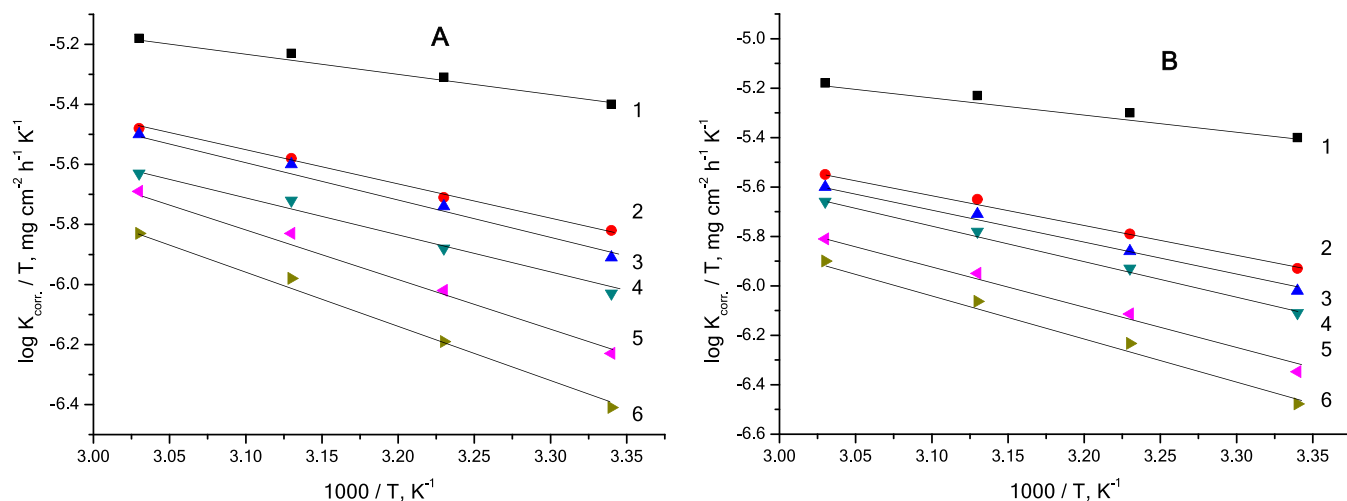


Figure 9. (A, B) Relationship between $\log K_{\text{corr}}/T$ and $1/T$ for the dissolution of X65CS in 1 M HCl solution alone and the existence of some concentrations of expired (A) BIF and (B) TER (1) 0.0 mg L⁻¹, (2) 75 mg L⁻¹, (3) 150 mg L⁻¹, (4) 225 mg L⁻¹, (5) 300 mg L⁻¹, and (6) 375 mg L⁻¹.

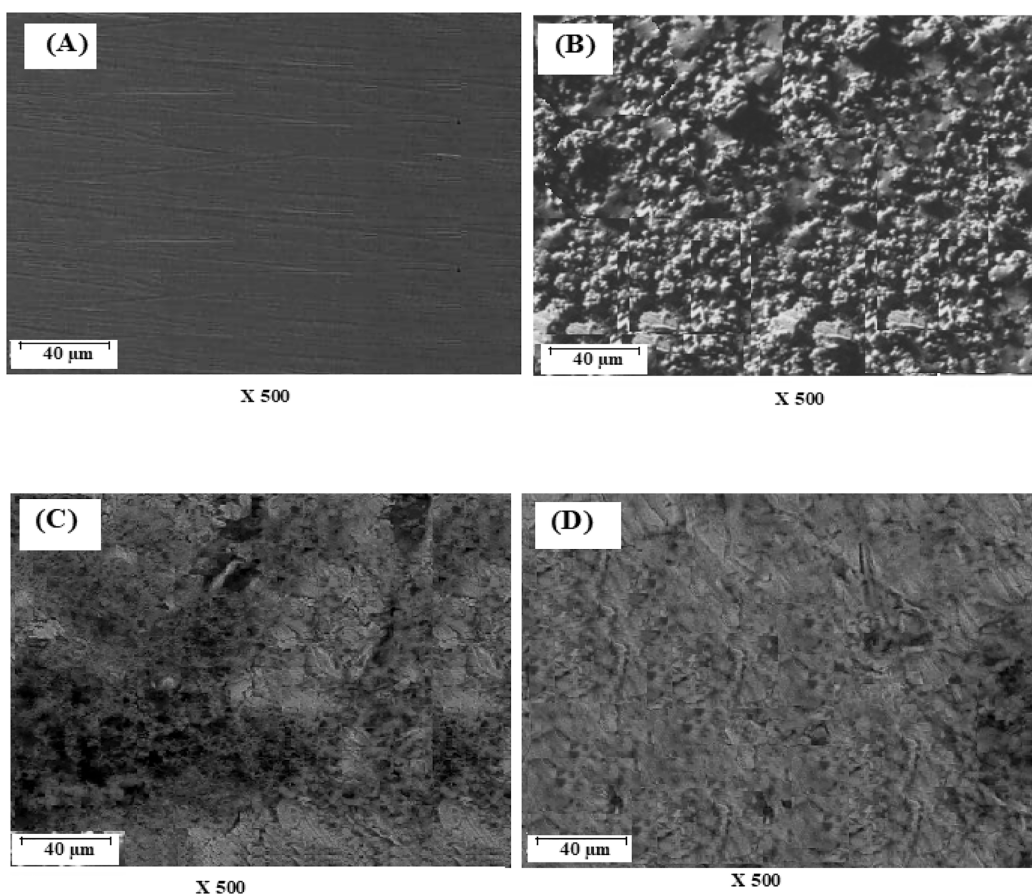


Figure 10. SEM micrographs of the X65CS surface (A) before immersion in 1 M HCl, (B) after immersion for an interval of 5 h in 1 M HCl solution, and (C) mixed with 375 ppm BIF and (D) 375 ppm TER at 25 °C.

$$T \Delta S_{\text{ads}} = \Delta H_{\text{ads}} - \Delta G_{\text{ads}} \quad (18)$$

The calculated ΔS_{ads} values for expired BIF were -0.086 , -0.081 , -0.073 , and -0.065 kJ mol⁻¹ at temperatures of 26, 36, 46, and 56 °C, respectively. The ΔS_{ads} values for expired TER were -0.069 , -0.064 , -0.057 , and -0.052 kJ mol⁻¹ at temperatures of 26, 36, 46, and 56 °C, respectively. The negative ΔS_{ads} values indicate that the disorder caused by the transition of the reactant to the adsorbent surface was

minimized. This confirms the strong adsorption of expired BIF and TER on the X65CS surface. The thermodynamic adsorption parameters correspond to a high % AE at lower temperatures.

All the corrosion functions acquired from the different techniques elucidate the inhibitory effect of expired BIF and TER. The % AE rises with rising concentrations of the expired drugs. Also, the anticorrosion could be explained by the blocking adsorption of the expired drugs on the X65CS owing to the fact

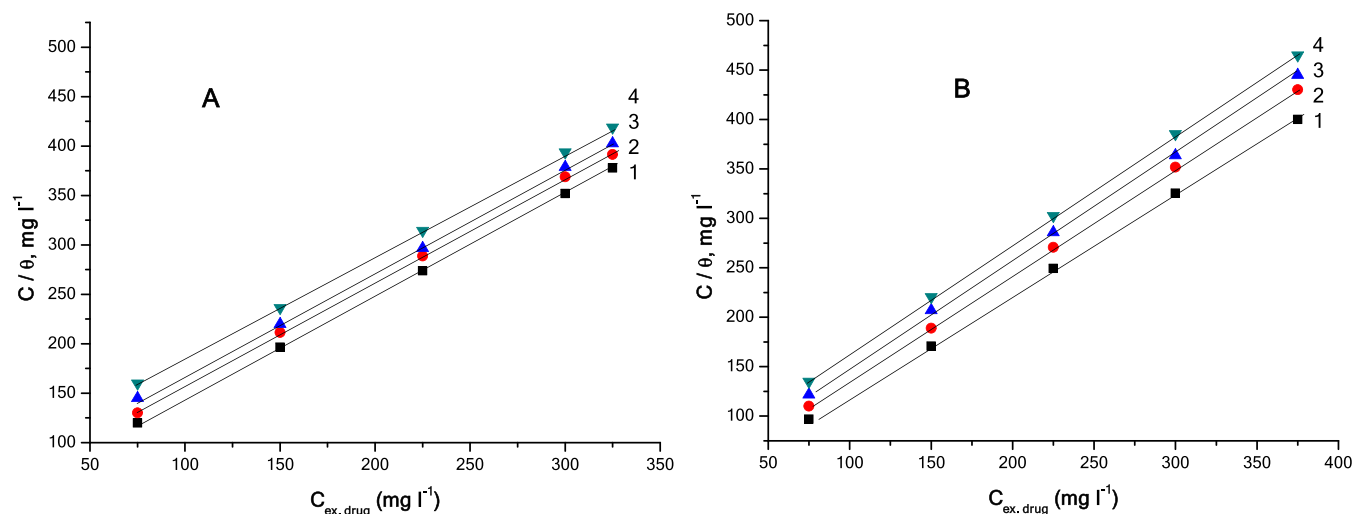


Figure 11. Langmuir isotherm plots for the X65CS in 1 M HCl including certain concentrations of expired (A) BIF and (B) TER at different temperatures. (1) 299 K, (2) 309 K, (3) 319 K, and (4) 329 K.

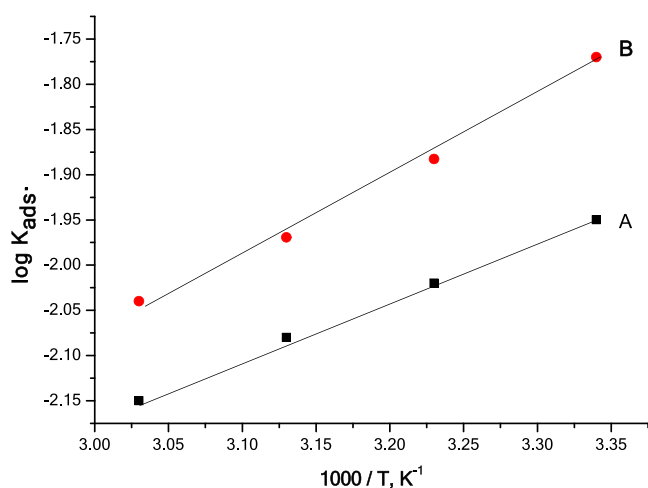


Figure 12. Relationship between $\log K_{\text{ads}}$ and $1000/T$ for the dissolution of X65CS in 1 M HCl solution in the presence of BIF and TER drugs at certain temperatures. (A) BIF and (B) TER.

that the values anodic and cathodic Tafel slopes are nearly constant. The % AE of expired TER is more than that obtained in expired BIF. These data can be interpreted because the molar mass of BIF ($310.40 \text{ g mol}^{-1}$) is less than the molar mass of TER ($532.47 \text{ g mol}^{-1}$). The height molar mass of TIR leads to a significant coverage of the adhesive layer on the surface of X65CS compared to that obtained in the case of the BIF layer. It

insulates the surface of the steel from the aggressive HCl solution and reduces the corrosion rate. Also, the existence of some active centers such as heterocyclic nitrogen atoms and oxygen in TER molecules compared with those obtained in BIF leads to more bonds sticking to the surface, and thus the % AE increases. Also, The TER molecule can form a more stable six-membered ring complex with Fe^{+2} on the CS surface than those obtained in BIF, leading to more bonds sticking to the surface and thus the % AE increases. Figure 13 shows the suggested schematic adsorption of the investigated inhibitors. The results of PDAP measurements demonstrate that the expired BIF and TER inhibits the pitting attack of X65CS in 1 M HCl solution containing Cl^- ions by moving the E_{pitt} to a more noble direction. The anti-corrosive strength of these expired drug originates from the competing adsorption between the Cl^- ions and the expired drugs on the X65CS surface until the expired drugs overcome the Cl^- ions, and thus the pitting attack of Cl^- ions is reduced.

3.7. DFT Study. The optimized geometries in the aqueous phase of the expired BIF and TER inhibitors are shown in Figure 14. The energy of the HOMO orbital (E_{HOMO}), as listed in Table 6, which increases as the donation process becomes more accessible, serves as a gauge of the anti-corrosive molecule's capacity to donate an electron to the steel surface. On the other hand, the energy of the LUMO orbital (E_{LUMO}), which gets low as the accepting process becomes easier, measures the ability of the inhibitor molecule to accept an electron from the steel surface. According to Table 6, the E_{HOMO} value of the TER

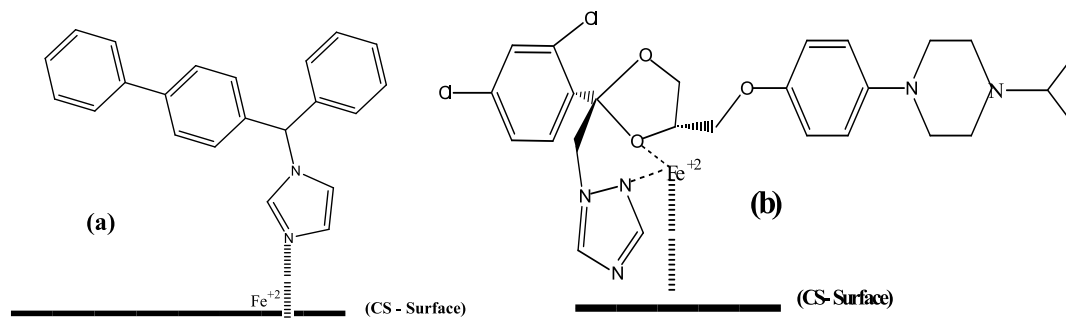
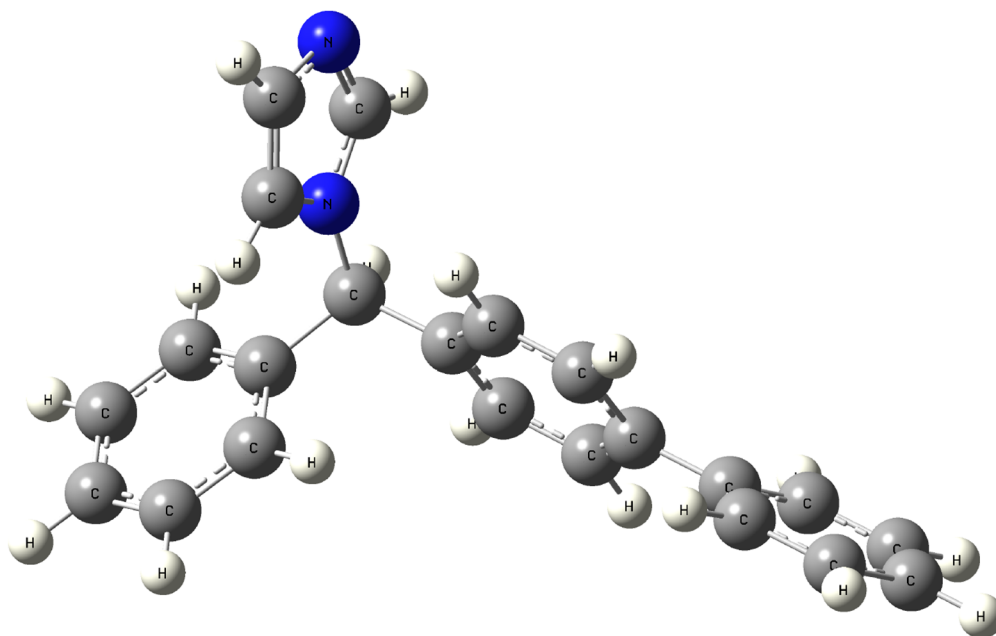


Figure 13. Schematic representation of the suggested adsorption of (a) BIF and (b) TER.

A



B

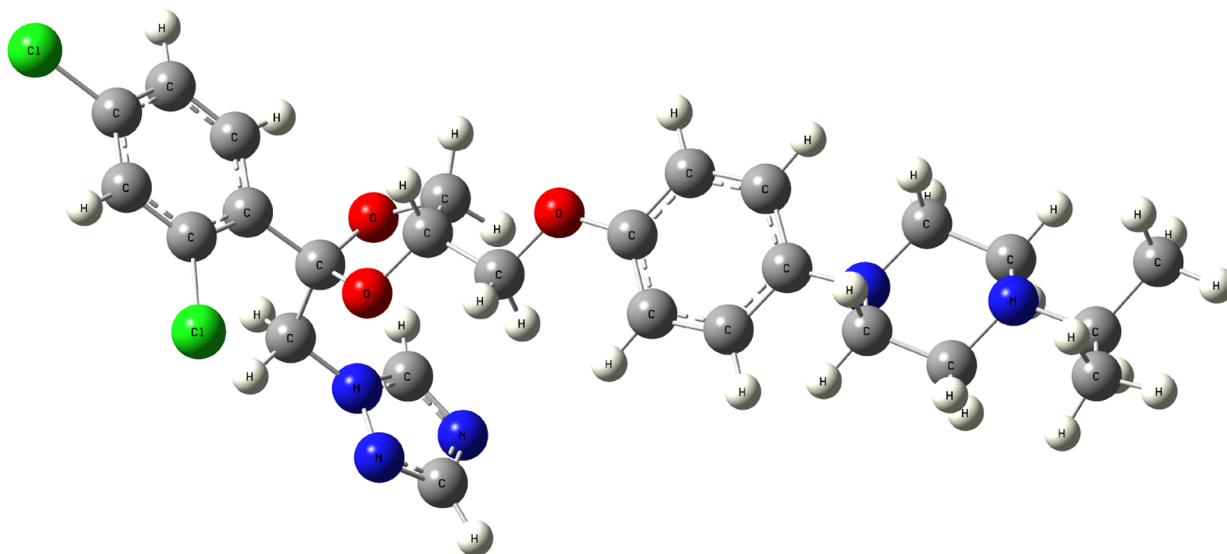


Figure 14. Optimized structures of (A) bifonazole and (B) terconazole inhibitors.

Table 6. Quantum Descriptors for Bifonazole and Terconazole Inhibitors

	HOMO (eV)	LUMO (eV)	ΔE (eV)	η (eV)	σ (eV ⁻¹)	ΔN (e)
bifonazole	-6.11545	-0.96133	5.154118	2.577059	0.388039	0.25
terconazole	-5.16827	-0.95344	4.214829	2.107415	0.474515	0.42

inhibitor becomes higher than that of the BIF inhibitor, and it would be expected that the ability to donate electrons becomes easier and the E_{LUMO} value of the TER inhibitor becomes lower than that of the BIF inhibitor. The obtained theoretical results coincide with experimental work where the TER inhibitor is a more reactive molecule toward an anti-corrosive behavior.

The energy gap (ΔE) is another substantial parameter, which was examined for the BIF and TER inhibitors. A correlation between the compound chemical reactivity to the X65CS

surface was found for the energy gap between HOMO and LUMO. The lower energy gap values will result in better inhibitory efficacy. Soft-base inhibitors are the most effective for metals. As listed in Table 6, the TER inhibitor has a smaller value of an energy gap than the BIF inhibitor, which demonstrated that the TER molecule is better than the BIF molecule as a corrosion inhibitor.

Global reactivity descriptors such as softness and hardness are fundamental chemical terms that have been theoretically

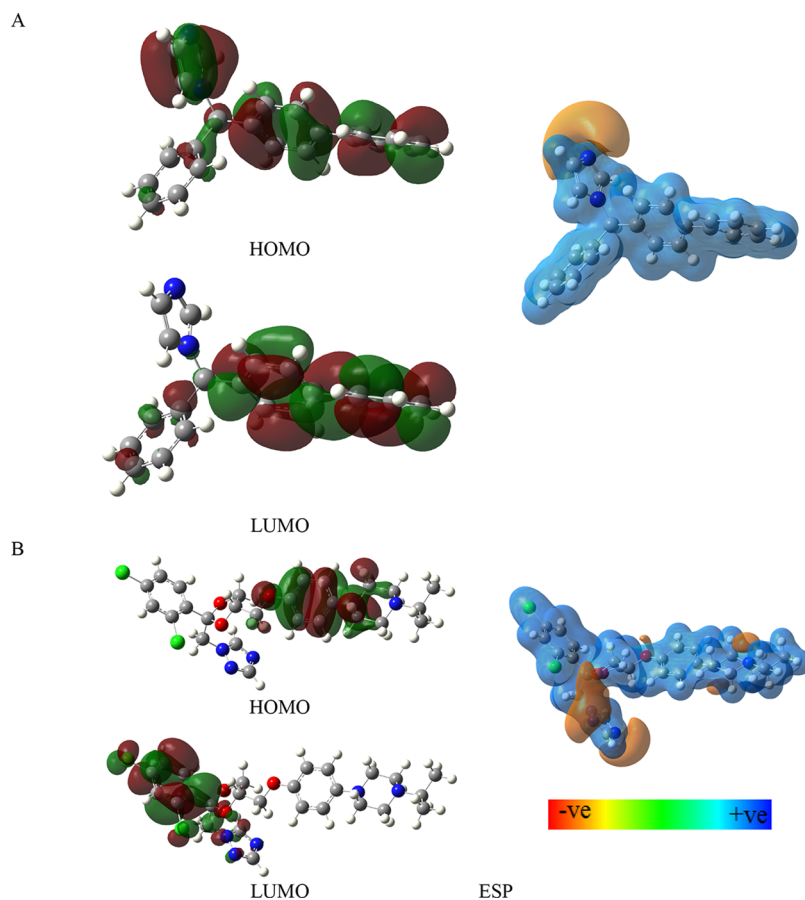


Figure 15. Frontier orbitals and ESP maps of (A) bifonazole and (B) terconazole molecules.

supported by density functional theory. These are crucial characteristics to gauge the reactivity and stability of molecules. The chemical hardness refers to the resistance to deformation or polarization of the electron cloud of the atoms, ions, or molecules under slight perturbation of a chemical reaction. A soft molecule has a small energy gap compared to a hard molecule that has a large energy gap.⁶¹ In general, anti-corrosive behavior with the highest global softness value and the lowest global hardness value is anticipated to have maximum inhibitory efficiency. Adsorption could take place at the region of the molecule where softness has the largest value. In the current investigation, as seen in Table 6, the TER molecule has a smaller hardness and higher softness, so the TER inhibitor is more effective toward anticorrosion than the BIF inhibitor.

To show which portions of the molecule are qualitatively capable of donating or accepting electrons, it is crucial to observe the unique distributions of HOMOs and LUMOs. As seen in Figure 15, the HOMOs for the BIF inhibitor is mainly distributed on the biphenyl and imidazole ring, and for the TER molecule, it is localized on the methoxyphenyl and piperazine ring. The LUMOs were localized on the biphenyl for BIF, and for TER, they are localized on the dichlorophenyl moiety.

Electrostatic potential maps (ESPs) are seen in Figure 15. It should be highlighted that a higher electron density in the red color zone is connected to the nucleophilic region.⁶² Due to the reduction of electrons, the blue area is the electrophilic site.⁶³ A nucleophilic site is located on the nitrogen and oxygen atoms for the TER inhibitor and on the nitrogen atom for BIF inhibitors. The electrophilic sites are on the whole molecules of both

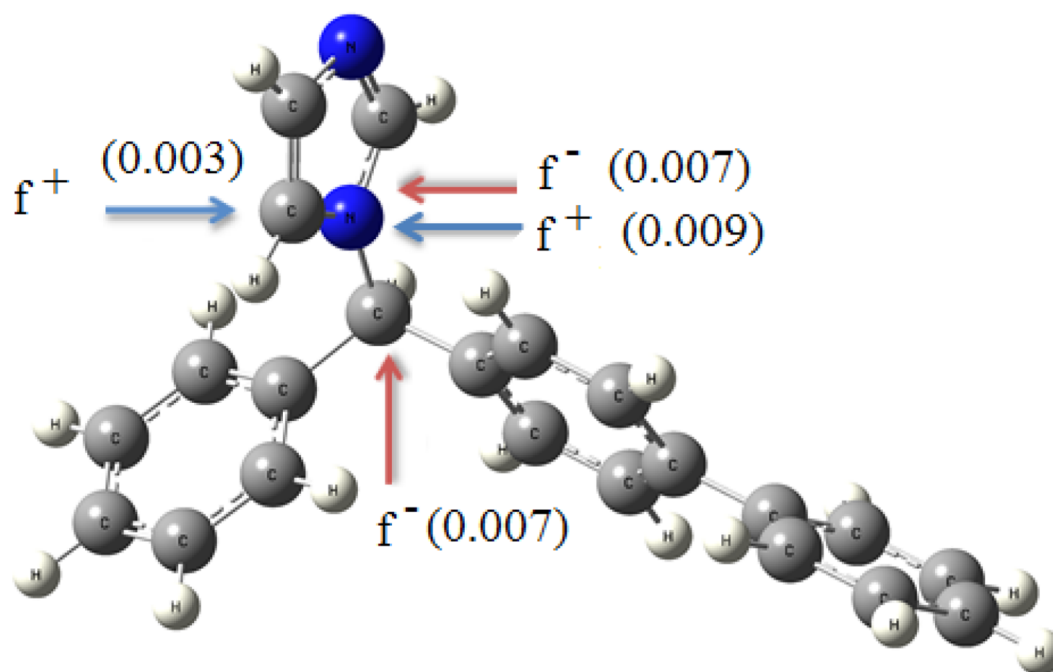
inhibitors. As a result, the adsorption of both expired drugs on the steel surface would be more reactive to nucleophilic attacks, resulting in the formation of an adsorbed film in the corrosion inhibition mechanism.

The literature claims that larger values of the electrons transferred (ΔN) support the high adsorption on the carbon steel surface, which provides the highest protection to steel. It is possible to quantify the electron transfer from the molecule to the metal surface if the fraction of electrons is more than zero.⁶³ The larger and positive results reported for TER (0.42e) and BIF (0.25e) inhibitors in this study, as listed in Table 6, are evidence of the major impact of both inhibitors for the transfer of electrons from the anti-corrosive to the steel surface.

Analysis of the condensed forms of the Fukui index was used to determine and identify local reactive sites in the compounds under study. As a result, the nucleophilic and electrophilic properties of the terconazole and bifonazole inhibitors were measured in order to predict the most active centers of the inhibitor molecules. The estimated Fukui indices for this notion in the aqueous phase are presented in Figure 16. The favored sites for the nucleophilic attack are the nitrogen atom of the imidazole ring for the bifonazole inhibitor and the carbon atom of dioxolan ring for the terconazole molecule. The favored sites for the electrophilic attack are the carbon that is bonded with nitrogen of the imidazole ring for the bifonazole and the carbon atom of the piperazine ring for the terconazole molecule.

3.8. MC Simulation. MC modeling was used for the interactions between the examined terconazole and bifonazole inhibitors and metallic surfaces (Fe(110)). Figure 17 depicts the top and side views of the stable adsorption formation of the

A



B

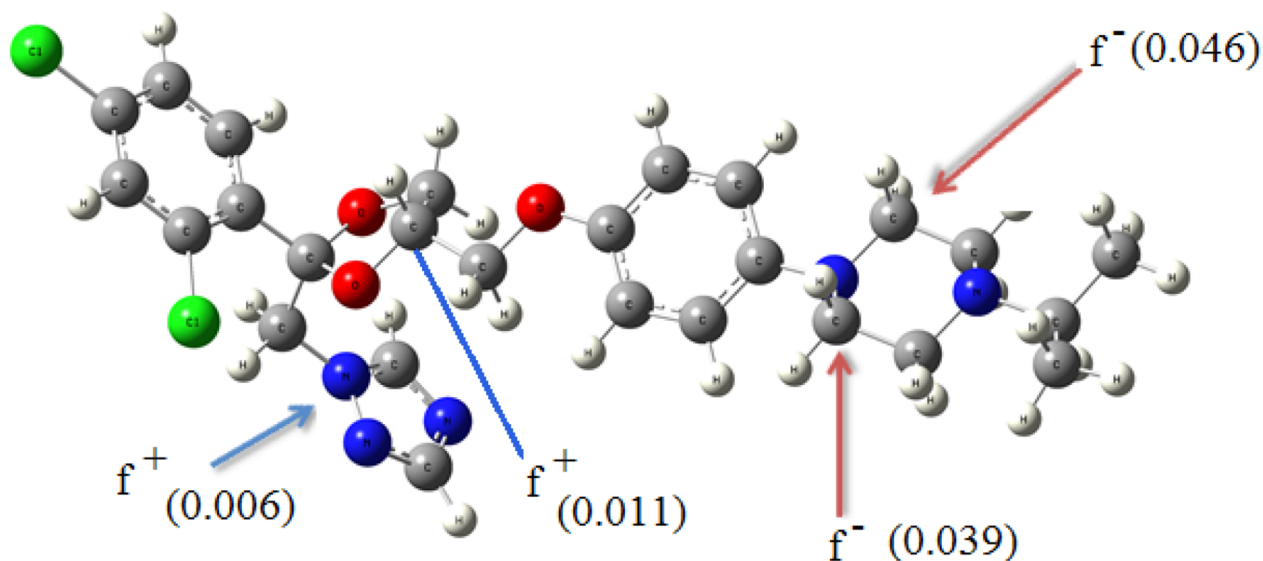


Figure 16. Fukui indices of the (A) bifonazole and (B) terconazole molecules.

terconazole and bifonazole inhibitors on the surface of Fe(110). The adsorption energies for terconazole and bifonazole inhibitor molecules on the Fe(110) surface are determined. The examined terconazole and bifonazole were positioned parallel to the metallic surface (Fe(110)), which increased their reactivity, as seen in Figure 17.

The evaluated E_{ads} values for terconazole and bifonazole are -154.22 and -94.43 kcal/mol, respectively (Table 7). The higher adsorption energy of the terconazole inhibitor demon-

strates that it is a more effective inhibitor than the bifonazole molecule.

4. CONCLUSIONS

Expired BIF and TER act as effective anticorrosion aid for general and pitting corrosion X65CS in 1 M HCl solution. The % AE increases with increasing the expired drug concentration and minimizing the temperature. The values of % AE reached 92.08 and 94.19% at 375 mg L^{-1} in the case of expired BIF and

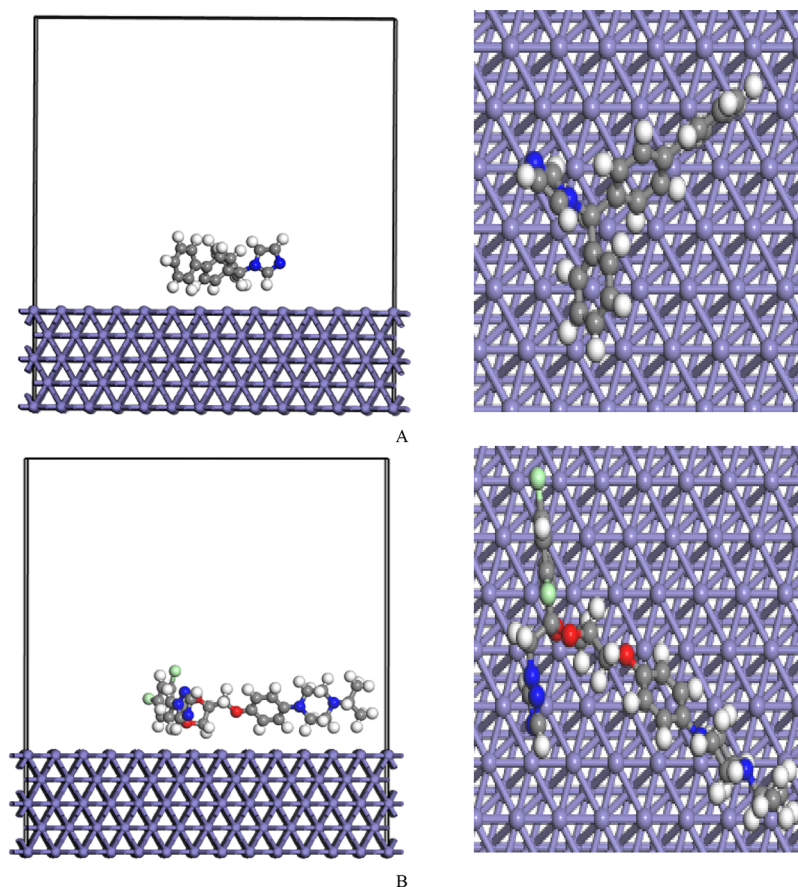


Figure 17. Top and side views of adsorbed (A) bifonazole and (B) terconazole on the Fe(110) surface.

Table 7. Adsorption Energies of the Bifonazole and Terconazole on the Fe(110) Surface

system	adsorption energy (kcal mol ⁻¹)
bifonazole + Fe(110)	-94.43
terconazole + Fe (110)	-154.22

TER, respectively, using polarization methods. The anti-corrosion process was explicated by the spontaneous adsorption of the expired BIF and TER on the X65CS surface to form an adsorbed film that isolates the steel surface from aggressive HCl solutions. The adsorption is subjected to the Langmuir isotherm. The outcomes obtained from all measurements indicate that the % AE of TER is higher than that of BIF, owing to the chemical structure and higher molar mass of TER. TER and BIF were studied using DFT and MC. The quantum parameters reveal that the TER inhibitor is more reactive than the BIF inhibitor. The adsorption of the two inhibitors on the Fe(110) is parallel to the surface.

AUTHOR INFORMATION

Corresponding Author

Metwally Abdallah – Chem. Depart. Faculty of Appl. Sci., Umm Al-Qura University, Mecca 21421, Saudi Arabia; orcid.org/0000-0002-6132-8849; Email: maabdelsaid@uqu.edu.sa

Authors

Kamal A. Soliman – Chem. Depart. Faculty of Sci., Benha University, Benha 13518, Egypt; orcid.org/0000-0001-8953-7709

Majda Alfakeer – Chem. Depart., College of Science, Princess Nourah bint Abdulrahman University, Riyadh 11564, Saudi Arabia

Hanaa Hawsawi – Chem. Depart. University College of Alwajh, Alwajh, University of Tabuk, Tabuk 71491, Saudi Arabia

Ameena Mohsen Al-bonayan – Chem. Depart. Faculty of Appl. Sci., Umm Al-Qura University, Mecca 21421, Saudi Arabia

Salih S. Al-Juaid – Chem. Depart., Faculty of Sci., King Abdulaziz University, Jeddah 21589, Saudi Arabia

Salah Abd El Wanees – Faculty College of Umluj, Umluj, University of Tabuk, Tabuk 71491, Saudi Arabia; Chemistry Department, Faculty of Science, Zagazig University, Zagazig 44519, Egypt

Mohamed S. Motawea – Chem. Depart. Faculty of Sci., Benha University, Benha 13518, Egypt; Chem. Depart., Faculty of Science, University of Tabuk, Tabuk 71491, Saudi Arabia

Complete contact information is available at:

<https://pubs.acs.org/10.1021/acsomega.3c03257>

Notes

The authors declare no competing financial interest.

ACKNOWLEDGMENTS

The authors extend their appreciation to the Deputyship for Research and Innovation, Ministry of Education in Saudi Arabia for funding this research work through the project no. IFP22UQU4320006DSR105.

REFERENCES

- (1) Jacob, K. S.; Parameswaran, G. Corrosion inhibition of mild steel in hydrochloric acid solution by Schiff base furoin thiosemicarbazone. *Corros. Sci.* **2010**, *52*, 224–228.
- (2) Issadi, S.; Douadi, T.; Zouaoui, A.; Chafaa, S.; Khan, M. A.; Bouet, G. Novel thiophine symmetrical Schiff base compounds as corrosion inhibitor for mild steel in acidic media. *Corros. Sci.* **2011**, *53*, 1484–1488.
- (3) Abdallah, M.; Asghar, B. H.; Zafarany, I.; Fouda, A. S. The Inhibition of Carbon Steel Corrosion in Hydrochloric Acid Solution using Some Phenolic Compounds. *Int. J. Electrochem. Sci.* **2012**, *7*, 282–304.
- (4) Jahdaly, B. A. A. L.; Awad, M. I.; Hazazi, O. A.; Shaaban, M. R.; Saad, A. F. Inhibition Efficiency of Some Amino Acids in the Presence of Vanillin for the Corrosion of Mild Steel in HCl Solution. *Int. J. Electrochem. Sci.* **2018**, *13*, 5284–5293.
- (5) Al Jahdaly, B. A.; Masaret, G. S. Synthesis and inhibitive behavior of new thiazolyl-pyrazole derivative at low carbon steel/HCl interface: Electrochemical, morphology and theoretical investigations. *J. Mol. Liq.* **2022**, *364*, No. 119933.
- (6) Masaret, G. S.; Jahdaly, B. A. A. Inhibitive and adsorption behavior of new thiazolidinone derivative as a corrosion inhibitor at mild steel/electrolyte interface: Experimental and theoretical studies. *J. Mol. Liq.* **2022**, *338*, No. 116534.
- (7) Awad, M. I.; Hazazi, O. A. Co-adsorption of a triazole derivative and copper ions on mild steel. *Prot. Met. Phys. Chem. Surf.* **2017**, *53*, 236–240.
- (8) Ahmed, S. A.; Awad, M. I.; Althagafi, I. I.; Altass, H. M.; Morad, M.; Alharbi, A.; Obaid, R. J. Newly synthesized indolium-based ionic liquids as unprecedented inhibitors for the corrosion of mild steel in acid medium. *J. Mol. Liq.* **2019**, *291*, No. 111356.
- (9) Abdallah, M.; Soliman, K. A.; Alfattani, R.; Al-Gorair, A. S.; Fawzy, A.; Ibrahim, M. A. A. Insight of corrosion mitigation performance of SABIC iron in 0.5 M HCl Solution by tryptophan and histidine: Experimental and computational approaches. *Int. J. Hydrogen Energy* **2022**, *47*, 12782–12797.
- (10) Abd El Wanees, S.; Al-Gorair, A. S.; Hawsawi, H.; Alotaibi, M. T.; Mahmoud, G. A.; Saleh, M. A.; Elyan, S. S. Inhibition of pitting corrosion of C-steel in oilfield-produced water using some purine derivatives. *Desalin. Water Treat.* **2022**, *269*, 21–32.
- (11) El-DougDoug, W. I.; Al-Gorair, A. S.; Elsaoud, A. A.; Hawsawi, H.; Elaraby, A.; Mabrouk, E. S.; Abdallah, M. Synthesis and assessment of Gemini cationic surfactants as inhibitors for corrosion of carbon steel in hydrochloric acid. *Green Chem. Lett. Rev.* **2022**, *15*, 796–812.
- (12) Laadam, G.; Benhiba, F.; El Faydy, M.; Titi, A.; Al-Gorair, A. S.; Alshareef, M.; Hawsawi, H.; Touzani, R.; Warad, I.; Bellaouchou, A.; Guenbour, M.; Abdallah, A. Anti-corrosion performance of novel pyrazole derivative for carbon steel corrosion in 1 M HCl: Computational and experimental studies. *Inorg. Chem. Comm.* **2022**, *145*, No. 109963.
- (13) Abdallah, M.; Soliman, K. A.; Alshareef, M.; Al-Gorair, A. S.; Hawsawi, H.; Altass, H. M.; Al-Juaid, S. S.; Motawea, S. M. Investigation of the anticorrosion and adsorption properties of two polymer compounds on the corrosion of SABIC iron in 1 M HCl solution by practical and computational approaches. *RSC Adv.* **2022**, *12*, 20122–20137.
- (14) Ahmed El Defrawy, M.; Abdallah, J. A.-F. Electrochemical and Theoretical Investigation for Some Pyrazolone Derivatives as Inhibitors for the Corrosion of C-Steel in 0.5 M Hydrochloric Acid. *J. Mol. Liq.* **2019**, *2019*, No. 110994.
- (15) Abdallah, M.; El Guesmi, N.; Al-Gorair, A. S.; El-Sayed, R.; Meshabi, A.; Sobhi, M. Enhancing the anticorrosion performance of mild steel in sulfuric acid using synthetic non-ionic surfactants: Practical and Theoretical Studies. *Green Chem. Lett. Rev.* **2021**, *14*, 381–393.
- (16) Hameed, R. S. A.; Al-Bagawi, A. H.; Shehata, H. A.; Shamroukh, A. H.; Abdallah, M. Corrosion Inhibition and Adsorption Properties of Some Heterocyclic Derivatives on C-Steel Surface in HCl. *J. Bio-Tribo-Corros.* **2021**, *51*, 1–11.
- (17) Abdel Hameed, S.; Alfakeer, M.; Abdallah, M. Inhibiting Properties of Some Heterocyclic Amide Derivatives as Potential Nontoxic Corrosion Inhibitors for Carbon Steel in 1-M Sulfuric Acid. *Surf. Eng. Appl. Electrochem.* **2018**, *54*, 599–606.
- (18) Abdel Hameed, R. S.; Abdallah, M. Corrosion Inhibition of Carbon Steel in 1M Hydrochloric Acid using some Pyrazolo[3,4-d]Pyrimidone Derivatives. *Prot. Met. Phys. Chem. Surf.* **2018**, *54*, 113–121.
- (19) Berrissoul, A.; Loukili, E.; Mechbal, N.; Benhiba, F.; Guenbour, A.; Dikici, B.; Zarrouk, A.; Dafali, A. Anticorrosion effect of a green sustainable inhibitor on mild steel in hydrochloric acid. *J. Colloid Interface Sci.* **2020**, *580*, 740–752.
- (20) Abdallah, M.; Soliman, K. A.; Al-Gorair, A. S.; Al Bahir, A.; Al-Fahemi, J. A.; Motawea, M. S.; Al-Juaid, S. S. Enhancing the inhibition and adsorption performance of SABIC iron corrosion in sulfuric acid by expired vitamins. Experimental and computational approach. *RSC Adv.* **2021**, *11*, 17092–17100.
- (21) Abdallah, M.; Al Bahir, A.; Altass, H. M.; Fawzy, A.; El Guesmi, N.; Al-Gorair, A.; Benhiba, F.; Warad, I.; Zarrouk, A. Anticorrosion and adsorption performance of expired antibacterial drugs on Sabc iron corrosion in HCl solution: Chemical, electrochemical and Theoretical Approach. *J. Mol. Liq.* **2021**, *330*, No. 115702.
- (22) Abdallah, M.; Hegazy, M. A.; Alfakeer, M.; Ahmed, H. Adsorption and inhibition performance of novel cationic Gemini surfactant as a safe corrosion inhibitor for carbon steel in hydrochloric acid. *Green Chem. Lett. Rev.* **2018**, *11*, 457–468.
- (23) Abdallah, M.; Fawzy, A.; Al Bahir, A. Expired amoxicillin and cefuroxime drugs as efficient anticorrosive for Sabc iron in 1-M hydrochloric acid solution. *Chem. Eng. Comm.* **2022**, *209*, 158–170.
- (24) Abdel Hameed, R. S.; Aleid, G. M. S.; Khaled, A.; Mohammad, D.; Enas, H.; Aljuhani, S.; Al-Mhyawi, R.; Freah Alshammery, M.; Abdallah, M. Expired Dulcolax Drug as Corrosion Inhibitor for Low Carbon Steel in Acidic Environment. *Int. J. Electrochem. Sci.* **2022**, *17*, 220655.
- (25) Abdel Hameed, R. S.; Obeidat, S.; Qureshi, M. T.; Al-Mhyawi, S. R.; Aljuhani, E. H.; Abdallah, M. Silver nanoparticles – expired medicinal drugs waste accumulated at Hail City for the local manufacturing of green corrosion inhibitor system for steel in acidic environment. *J. Mater. Res. Technol.* **2022**, *21*, 2743–2756.
- (26) Haruna, K.; Saleh, T. A.; Quraishi, M. A. Expired metformin drug as green corrosion inhibitor for simulated oil/gas well acidizing environment. *J. Mol. Liq.* **2020**, *315*, No. 113716.
- (27) Abdallah, M.; Soliman, K. A.; Al-Gorair, A. S.; Al Bahir, A.; Al-Fahemi, J. H.; Motawea, M. S.; Al-Juaid, S. S. Enhancing the inhibition and adsorption performance of SABIC iron corrosion in sulfuric acid by expired vitamins. Experimental and computational approach, *RSC. Advances* **2021**, *11*, 17092–17107.
- (28) Zakaria, K.; Abbas, M. A.; Bedair, M. A. Herbal expired drug bearing glycosides and polysaccharides moieties as green and cost-effective oilfield corrosion inhibitor: Electrochemical and computational studies. *J. Mol. Liq.* **2022**, *352*, No. 118689.
- (29) Elabbasym, H. M.; Gadaw, H. S. Study the effect of expires tenoxicam on the inhibition of carbon steel corrosion in a solution of hydrochloric acid. *J. Mol. Liq.* **2021**, *321*, No. 114918.
- (30) Abdallah, M.; Fawzy, A.; Alfakeer, M.; Altass, H. M. Expired Azithromycin and Roxithromycin Drugs as Environmentally Friendly Inhibitors for Mild Steel Corrosion in H₂SO₄ Solutions. *Green Chem. Lett. Rev.* **2021**, *14*, 509–518.
- (31) Saraswat, V.; Yadav, M.; Obot, I. B. Investigations on eco-friendly corrosion inhibitors for mild steel in acid environment: Electrochemical, DFT and Monte Carlo Simulation approach. *Colloids Surf, A* **2020**, *599*, No. 124881.
- (32) Mashuga, M. E.; Olanunmi, L. O.; Lgaz, H.; Sherif, E.-S. M.; Ebenso, E. E. Aminomethylpyridazine isomers as corrosion inhibitors for mild steel in 1 M HCl: Electrochemical, DFT and Monte Carlo simulation studies. *J. Mol. Liq.* **2021**, *344*, No. 117882.
- (33) Paul, P. K.; Yadav, M. Investigation on corrosion inhibition and adsorption mechanism of triazine-thiourea derivatives at mild steel /

HCl solution interface: Electrochemical, XPS, DFT and Monte Carlo simulation approach. *J. Electroanal. Chem.* **2020**, *877*, No. 114599.

(34) Mathur, P. B.; Vasudevan, T. Reaction-rate studies for the corrosion of metals in acids: iron in mineral acids. *Corrosion* **1982**, *38*, 17–25.

(35) Barone, V.; Cossi, M. Quantum Calculation of Molecular Energies and Energy Gradients in Solution by a Conductor Solvent Model. *J. Phys. Chem. A* **1998**, *102*, 1995–2001.

(36) Frisch, M. J.; Trucks, G. W.; Schlegel, H. B.; Scuseria, G. E.; Robb, M. A.; Cheeseman, J. R.; Scalmani, G.; Barone, V.; Mennucci, B.; Petersson, G. A.; Nakatsuji, H.; Caricato, M.; Li, X.; Hratchian, H. P.; Izmaylov, A. F.; Bloino, J.; Zheng, G.; Sonnenberg, J. L.; Hada, M.; Ehara, M.; Toyota, K.; Fukuda, R.; Hasegawa, J.; Ishida, M.; Nakajima, T.; Honda, Y.; Kitao, O.; Nakai, H.; Vreven, T.; Montgomery, J. A.; Peralta, J. E.; Ogliaro, F.; Bearpark, M.; Heyd, J. J.; Brothers, E.; Kudin, K. N.; Staroverov, V. N.; Kobayashi, R.; Normand, J.; Raghavachari, K.; Rendell, A.; Burant, J. C.; Iyengar, S. S.; Tomasi, J.; Cossi, M.; Rega, N.; Millam, J. M.; Klene, M.; Knox, J. E.; Cross, J. B.; Bakken, V.; Adamo, C.; Jaramillo, J.; Gomperts, R.; Stratmann, R. E.; Yazyev, O.; Austin, A. J.; Cammi, R.; Pomelli, C.; Ochterski, J. W.; Martin, R. L.; Morokuma, K.; Zakrzewski, V. G.; Voth, G. A.; Salvador, P.; Dannenberg, J. J.; Dapprich, S.; Daniels, A. D.; Farkas, J. B. F.; Ortiz, J. V.; Cioslowski, J.; Fox, D. J. *Gaussian 09*, Gaussian, Inc., Wallingford CT, 2009.

(37) Saraçoglu, M.; Elusta, M. I. A.; Kaya, S.; Kaya, C.; Kandemirli, F. Quantum chemical studies on the corrosion inhibition of Fe78B13Si9 glassy alloy in Na2SO4 solution of some thiosemicarbazone derivatives. *Int. J. Electrochem. Sci.* **2018**, *13*, 8241–8259.

(38) Douche, D.; Elmsellem, H.; Anouar, E. H.; Guo, L.; Hafez, B.; Tüzün, B.; El Louzi, A.; Bougrin, K.; Karrouchi, K.; Himmi, B. Anti-corrosion performance of 8-hydroxyquinoline derivatives for mild steel in acidic medium: gravimetric, electrochemical, DFT and molecular dynamics simulation investigations. *J. Mol. Liq.* **2020**, *308*, No. 113042.

(39) Sahin, M.; Gece, G.; Karc, M.; Bilgic, S. Experimental and theoretical study of the effect of some heterocyclic compounds on the corrosion of low carbon steel in 3.5% NaCl medium. *J. Appl. Electrochem.* **2008**, *38*, 809–815.

(40) Olasunkanmi, L. O.; Aniki, N. I.; Adekunle, A. S.; Durosinmi, L. M.; Durodola, S. S.; Wahab, O. O.; Ebenso, E. E. Investigating the synergism of some hydrazinecarboxamides and iodide ions as corrosion inhibitor formulations for mild steel in hydrochloric Acid: Experimental and computational studies. *J. Mol. Liq.* **2021**, *343*, No. 117600.

(41) Abdallah, M.; Altass, H. M.; Al-Gorair, A. S.; Al-Fahemi, J. H.; Soliman, K. A. Natural nutmeg oil as a green corrosion inhibitor for carbon steel in 1-M HCl solution: Chemical, electrochemical and computational methods. *J. Mol. Liq.* **2021**, *323*, No. 115036.

(42) Li, X.; Deng, S.; Fu, H. Allyl thiourea as a corrosion inhibitor for cold rolled steel in H3PO4 solution. *Corros. Sci.* **2012**, *55*, 280–288.

(43) Lebrini, M.; Bentiss, F.; Vezin, H.; Lagrenée, M. The inhibition of mild steel corrosion in acidic solutions by 2,5-bis(4-pyridyl)-1,3,4-thiadiazole: Structure–activity correlation. *Corros. Sci.* **2006**, *48*, 1279–1291.

(44) Sobhi, M. A.; Al Tass, H. M. Corrosion inhibition of aluminum in hydrochloric acid by pyrazinamide derivatives. *J. Mol. Liq.* **2016**, *223*, 1143–1150.

(45) Mahdavian, M.; Ashhari, S. Corrosion inhibition performance of 2-mercaptopbenzimidazole and 2-mercaptobenzoxazole compounds for protection of mild steel in hydrochloric acid solution. *Electrochim. Acta* **2010**, *55*, 1720–1724.

(46) Abdallah, M.; Al Karane, S. A.; Abdel Fattah, A. A. Inhibition of the corrosion of nickel by natural black cummin oil. *Chem. Eng. Comm.* **2010**, *197*, 1446–1454.

(47) Abdallah, M.; Fawzy, A.; Hawsawi, H.; Abdel Hameed, R. S.; Al-Juaid, S. S. Estimation of Water-Soluble Polymers (Plaxamer and Pectin) as Corrosion Inhibitors for Carbon Steel in Acidic Medium. *Int. J. Electrochem. Sci.* **2020**, *15*, 8129–8144.

(48) Sobhi, M.; Abdallah, M.; Khairou, K. S. Sildenafil citrate (Viagra) as a corrosion inhibitor for carbon steel in hydrochloric acid solutions. *Monatsh. Chem.* **2012**, *143*, 1379–1387.

(49) Abdallah, M.; Hatem, M.; Hegazy, E. M. A.; Ahmed, H. Adsorption and inhibition effect of novel cationic surfactant for pipelines carbon steel in acidic solutions. *Prot. Met. Phys. Chem. Surf.* **2016**, *52*, 721–730.

(50) Riggs, O. L., Jr.; Hurd, R. M. Temperature coefficient of corrosion inhibition. *Corrosion* **1967**, *23*, 252–258.

(51) Laider, K. G. *Chemical Kinetics*, Mc Graw Hill Publishing Company Ltd, 1965.

(52) Abdallah, M.; Alfakeer, M.; Al-Gorair, A. S.; Al Bahir, A.; Sobhi, M. Enhancing the inhibition effect and adsorption efficiency of ethoxylated dodecyl alcohols on corrosion of 316 stainless steels in 2M HCl. *Int. J. Electrochem. Sci.* **2021**, *16*, 210622.

(53) Abdallah, M.; Alfakeer, M.; Alonazi, A. M.; Al-Juaid, S. S. Ketamine drug as an inhibitor for the corrosion of 316 stainless steel in 2M HCl solution. *Int. J. Electrochem. Sci.* **2019**, *14*, 10227–10247.

(54) Salhi, A.; Tighadouini, S.; El-Massaoudi, M.; Elbelghiti, M.; Bouyanzer, A.; Radi, S.; El Barkany, S.; Bentiss, F.; Zarrouk, A. Ketone heterocycles as new compounds of corrosion inhibitors for carbon steel in 1 M HCl: weight loss, electrochemical and quantum chemical investigation. *J. Mol. Liq.* **2017**, *248*, 340–349.

(55) Farag, A. A.; Eid, A. M.; Shaban, M. M.; Mohamed, E. A.; Raju, G. Integrated modeling, surface, electrochemical, and biocidal investigations of novel benzothiazoles as corrosion inhibitors for shale formation well stimulation. *J. Mol. Liq.* **2021**, *336*, No. 116315.

(56) Döner, A.; Şahin, E. A.; Kardaş, G.; Serindağ, O. Investigation of corrosion inhibition effect of 1,1'-thiocarbonyldiimidazole on mild steel in hydrochloric acid solution. *Prot. Met. Phys. Chem. Surf.* **2011**, *47*, 264–271.

(57) Ahamad, I.; Prasad, R.; Quraishi, M. A. Inhibition of mild steel corrosion in acid solution by Pheniramine drug: Experimental and theoretical study. *Corros. Sci.* **2010**, *52*, 3033–3041.

(58) Solmaz, R. Investigation of adsorption and corrosion inhibition of mild steel in hydrochloric acid solution by 5-(4-Dimethylaminobenzylidene)rhodanine. *Corros. Sci.* **2014**, *79*, 169–176.

(59) Fawzy, A.; Zaafarany, I. A.; Ali, H. M.; Abdallah, M. New Synthesized Amino Acids-based Surfactants as efficient inhibitors for corrosion of mild Steel in hydrochloric acid medium: Kinetics and thermodynamic approach. *Int. J. Electrochem. Sci.* **2018**, *13*, 4575–4600.

(60) Obi-Egbedi, N. O.; Obot, I. B.; El-khaiary, M. I.; Umoren, S. A.; Ebenso, E. E. Computational Simulation and Statistical Analysis on the Relationship Between Corrosion Inhibition Efficiency and Molecular Structure of Some Phenanthroline Derivatives on Mild Steel Surface. *Int. J. Electrochem. Sci.* **2011**, *6*, 5649–5675.

(61) Demir, S.; Cakmak, S.; Dege, N.; Odabasoglu, M.; Aysun Kepekci, R.; Kutuk, H. A Novel 3-Acetoxy-2-methyl-N-(4-methoxyphenyl)benzamide: Molecular Structural Describe, Antioxidant Activity with Use X-ray Diffractions and DFT Calculations. *J. Mol. Struct.* **2015**, *1100*, 582–591.

(62) Viana, R. B.; Ribeiro, G. L. O.; Santos, G. L. O.; Sinara, F. F.; Quintero, D. E.; Viana, A. B.; Da Silva, A. B. F.; Moreno-Fuquen, R. Intramolecular interactions, isomerization and vibrational frequencies of two paracetamol analogues: a spectroscopic and a computational approach. *Spectrochim. Acta. Mol. Biomol. Spectr.* **2016**, *162*, 16–26.

(63) Dkhireche, N.; Galai, M.; Ouakki, M.; Rbaa, M.; Ech-chihbi, E.; Lakhri, B.; Touhami, M. E. Electrochemical and theoretical study of newly quinoline derivatives as a corrosion inhibitors adsorption on mild steel in phosphoric acid media. *Inorg. Chem. Commun.* **2020**, *121*, No. 108222.